Joint Transceiver Optimization for DF Multicasting MIMO Relay Systems with Wireless Information and Power Transfer

Shuche Wang, Zhiqiang He, *Member, IEEE*, and Yue Rong, *Senior Member, IEEE*

***Abstract*—In this article, we investigate a two-hop decode-and-forward (DF) multicasting multiple-input multiple-output (MIMO) wireless relay communication system. Different to conventional systems, the radio frequency (RF) energy from the source node is harvested at the relay node and used for forwarding signals to a group of receivers. Considering the structure of the energy harvesting (EH) relay node, we present a power splitting (PS) based protocol and a novel time switching (TS) based protocol by introducing two additional TS factors. For both protocols, we maximize the system mutual information (MI) of the multicasting MIMO relay system by jointly optimizing the source and relay covariance matrices under the constraints of the source energy and the relay harvested energy. In addition, a practical nonlinear EH model is adopted, where the energy harvested by the relay node is bounded as the incident RF signal power increases, and the harvested power is zero when the input power is below the minimum power for harvesting. For the TS based protocol, we also consider peak transmission power constraints at both the source and relay nodes. The performance of the proposed algorithms is verified via numerical simulations. The results demonstrate that the novel TS based protocol achieves a larger MI than the conventional TS protocol. The PS and TS based protocols achieve tradeoffs at different source power levels. In particular, compared with the PS based protocol, the proposed novel TS based protocol can reach a higher system MI when the EH bound is not reached, while the former protocol reaches a higher MI when the EH circuit is saturated. We show that the peak harvested energy constraint plays an important role in selecting the optimal location of the relay node.**

***Index Terms*—Decode-and-forward, MIMO-relay, multicasting, power-splitting, simultaneous wireless information and power transfer (SWIPT), time-switching.**

I. Introduction

The fifth generation (5G) communication network is expected to support intelligent devices with a higher rate and capacity but reduced energy consumption. To achieve this requirement, it is necessary to provide these devices with a consistent and stable energy supply. However, the power of many devices is supplied by batteries with a limited lifetime, and it is difficult and costly to replace depleted batteries in many applications. Therefore, energy harvesting (EH) from the environment is considered as an attracting technology in the 5G communication network.

A key factor of an EH communication system is how to efficiently harvest energy. Most of the conventional EH methods rely on natural resources [1], [2]. The radio frequency (RF) based EH techniques are treated as an alternative to that of conventional methods [3].

Meanwhile, facing with practical demands, one source node is often required to transmit common information to a number of receivers simultaneously, which is named as multicasting. In recent years, wireless multicasting technology has attracted numerous interests in 5G communication systems, which is used for streaming media over the Internet, like live TV and Internet radio.

A. Related Works

An ideal receiver which can perform EH and information decoding simultaneously has been investigated in [4]. Two main types of EH architecture have been proposed in practice [3]. The first type is the power splitting (PS) protocol, where one portion of the received signal is for EH and the remaining one is for information processing or information transmission. The other type is the time switching (TS) protocol, which performs wireless power transfer (WPT) and wireless information transfer (WIT) at different time intervals [5].

Cooperative relay communication is an important technique to enhance the system reliability and coverage [6]. Thus, wireless cooperative relay communication via simultaneous wireless information and power transfer (SWIPT) is an interesting concept [7]-[25]. In [7], a two-hop single-input single-output (SISO) amplify-and-forward (AF) relay system with PS and TS protocols has been considered. The authors of [7] analyzed the channel capacity and the outage probability under the system delay constraints. A dual-hop SISO orthogonal frequency-division multiplexing (OFDM) decode-and-forward (DF) relay system has been studied via a PS based protocol in [8]. In [9], a DF relay system with randomly located nodes has been studied. It has been proven in [9] that EH relay nodes can obtain the same diversity gain compared with conventional self-powered relays. In [10], the energy efficiency optimization of a distributed antenna system with SWIPT has been investigated.

Multiple-input multiple-output (MIMO) techniques have shown the advantages in increasing the energy and spectral efficiency of SWIPT systems. In [5], a one-hop MIMO broadcasting system has been studied, where receivers implement

This work was supported by the National Key Research and Development Program of China under Grant 2018YFB1801101.

S. Wang and Z. He are with the Key Laboratory of Universal Wireless Communications, Ministry of Education, Beijing University of Posts and Telecommunications, Beijing, China (e-mails: wangsc@bupt.edu.cn; hezq@bupt.edu.cn).

Y. Rong is with the School of Electrical Engineering, Computing and Mathematical Sciences, Curtin University, Bentley, WA 6102, Australia (e-mail: y.rong@curtin.edu.au).

EH and information decoding separately. Energy-rate tradeoffs in SWIPT MIMO systems have been revealed in [5]. A SWIPT massive MIMO system with the combination of multiple users and hybrid data-and-energy access point has been studied in [11] and [12]. In [13], transmit precoding and receive power splitting in MIMO SWIPT systems have been investigated with the aim to maximize the harvested power under the quality-of-service requirement of the MIMO link.

SWIPT MIMO relay systems have been studied in [1], [14]-[22]. Challenges and trade-offs of the SWIPT technology have been analyzed in [1]. In [14], a two-hop MIMO relay system with a multi-antenna EH receiver has been investigated, where the source and relay nodes use space-time block codes for information transmission. Moreover, jointly optimal source and relay precoders have been designed in [14] to obtain trade-offs between energy and information transmission. In [15], an antenna switching policy has been investigated in a DF MIMO relay system where the strongest antennas are used for information decoding while others are used for EH. In [16] and [17], TS based full-duplex relay systems have been studied. It has been shown that for both the TS and PS based protocols, there is a higher system throughput than the half-duplex architecture.

A practical two-phase MIMO-OFDM communication system with a wireless-powered full-duplex relay has been considered in [18], where a dedicated energy source is placed for the relay node to harvest sufficient energy. Furthermore, jointly optimal source and relay precoding matrices design in SWIPT AF MIMO relay systems to maximize the system data rate has been studied in [19]-[21]. In [22], the optimal source and relay matrices design has been discussed for a SWIPT DF MIMO relay system. The channel estimation error in a SWIPT DF MIMO relay system has been considered in [23], where the impact of imperfect channel state information (CSI) on the achievable transmission rate and the harvested energy has been analyzed. In [24], a robust beamforming scheme for SWIPT-aided relay systems in the presence of eavesdropper and imperfect CSI has been studied. A relay-assisted downlink massive MIMO system with SWIPT has been proposed in [25], where the method of CSI acquisition in the base station has been investigated. It is worth noting that the existing works [14]-[25] do not consider a DF multicasting MIMO relay system with a wireless powered relay node.

B. Contributions

In this paper, we investigate a dual-hop DF multicasting MIMO relay system with SWIPT, where the source node first sends energy-carrying and information-bearing signals to the relay node. Then by using the harvested energy, the received information signal is decoded at the relay node, re-encoded into new signal, and multicast to multiple receivers. Taking into account the limited energy harvesting capacity of the EH relay node, our system is mainly considered to be applied in low-rate multicasting scenarios, where multiple receivers (users) request low-rate data transmission from the source node at the same time. Considering the structure of the EH relay node, we present both the PS based protocol and a novel TS based protocol by introducing two additional TS factors. We investigate the optimal source covariance matrix and relay covariance matrix design to maximize the system mutual information (MI). To the best of our knowledge, this is the first paper studying DF multicasting MIMO relay systems with a wireless powered relay node. The main contributions of this paper in comparison to existing works are summarized below:

- Different to the conventional TS protocol [19]-[23], we propose a novel TS based protocol for MIMO DF multicasting relay systems. In addition to the TS factor for the energy transfer, we introduce two new TS factors for the information transmission. This enables us to optimize the time allocation between two hops of information transmission, which can achieve up to 60% higher system MI compared with the existing TS protocol, as indicated by the simulation results.
- Based on the proposed new TS protocol, we jointly optimize the source covariance matrix, the relay covariance matrix, and the three TS factors to maximize the system MI between the source node and receivers under the source energy constraints at the source node and the peak harvested energy constraint at the relay node. To prevent the transmission power of the source node and the relay node from approaching a very large value when the TS factors are small, the maximal transmission power limits are included at both the source and relay nodes.
- Compared with [19]-[23], a more practical nonlinear EH model is applied at the relay node. In this model, the harvested energy is bounded as the incident RF signal power increases, and the harvested power is zero when the input power is below the minimum power for harvesting (i.e., limited harvesting sensitivity). In addition, we consider the circuit energy consumption at the relay node.
- For the PS based protocol, in order to maximize the system MI, we investigate the joint design of the PS factor, the source covariance matrix, and the relay covariance matrix under constraints of the source power and the harvested energy at the relay node.
- The performance of the proposed SWIPT DF multicasting MIMO relay systems is assessed by numerical simulations. It can be seen that the TS based protocol and the PS based protocol achieve tradeoffs at different source power levels. In particular, the proposed novel TS protocol has a higher system MI than the PS based protocol when the bound of the harvested energy is not reached. When the EH circuit is saturated, the PS protocol can obtain a higher system MI compared with the TS based protocol. We show that the peak harvested energy constraint has a great impact on selecting the optimal location of the relay node.

C. Structure

The remainder of this article is outlined as follows. Section II presents the model of a dual-hop DF multicasting MIMO relay system with an EH relay node. Following that, the optimization problems for maximizing the MI based on

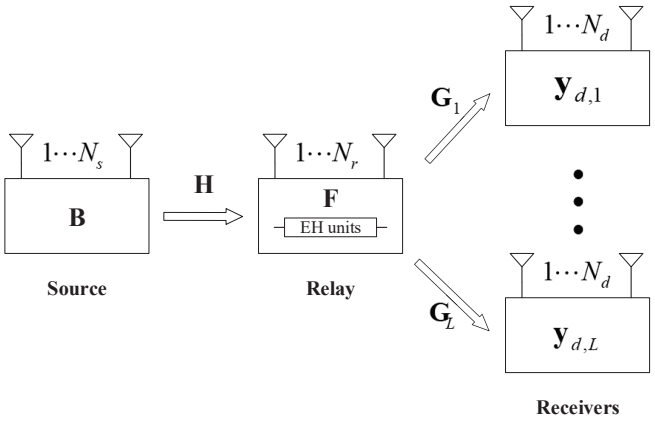

Fig. 1: Block diagram of a dual-hop DF multicasting MIMO relay system with an EH relay node.

both the PS and the proposed TS protocols are developed in this section. Section III depicts the proposed algorithms for solving the optimization problems. In Section IV, numerical simulations are shown to verify the performance of the proposed DF multicasting MIMO relay system. Finally, conclusions are drawn in Section V.

II. System model

In this paper, a dual-hop DF multicasting MIMO relay system with multiple receivers is investigated, where the source node simultaneously multicasts information to L receivers via the help of an EH relay node as illustrated in Fig. 1. There are N_s and N_r antennas at the source node and the relay node, respectively. For simplicity, the number of antennas at each receiver is assumed to be N_d. Moreover, the source node is assumed to have a stable power supply, while the relay node needs to harvest the RF energy transmitted by the source node. Similar to [14], [19], [26], in this paper, we do not consider the direct links between the source node and receivers since the direct links suffer from much more severe path attenuation than links through the relay node. We will discuss three protocols for a DF multicasting MIMO relay system: The proposed TS protocol with and without maximal transmission power limits and the PS based protocol.

A. The TS Based Protocol

In this paper, we consider the relay system is half-duplex. For the TS based protocol, it can be seen from Fig. 2a that the time of one communication period T from the source node to receivers is divided into three intervals. During the first interval of αT, the source node transmits an $N_s \times 1$ RF energy-carrying signal vector $\mathbf{s}_1$ to the relay node, where $0 < \alpha < 1$ stands for the TS factor in the first interval. We assume that $E\{\mathbf{s}_1\mathbf{s}_1^H\} = \mathbf{P}_1$, where $E\{\cdot\}$ is the statistical expectation and $(\cdot)^H$ stands for the Hermitian transpose. The received signal vector at the relay node can be shown as

$$\mathbf{y}_{r,1} = \mathbf{H}\mathbf{s}_1 + \mathbf{v}_{r,1} \tag{1}$$

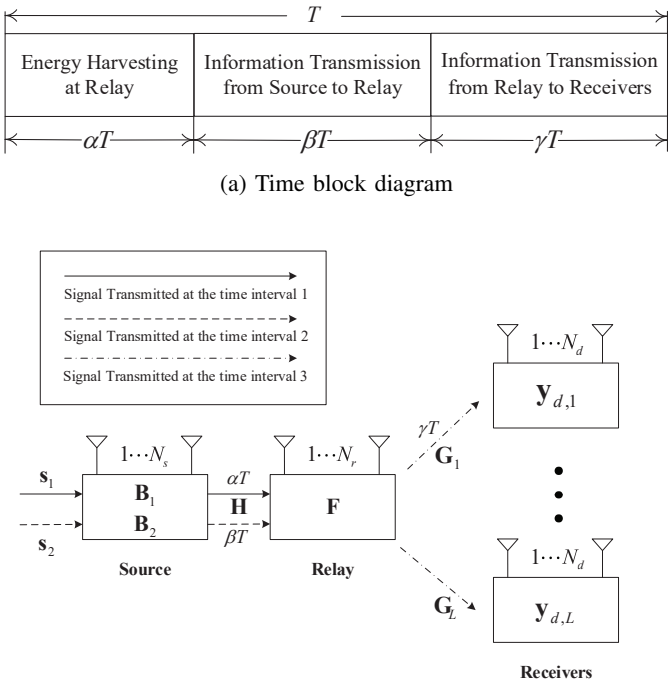

(a) Time block diagram

(b) System block diagram

Fig. 2: The proposed TS based protocol.

where $\mathbf{H}$ denotes the $N_r \times N_s$ source-relay channel matrix and vector $\mathbf{v}_{r,1}$ denotes the additive Gaussian noise at the relay at the first time slot.

For the linear EH model [5], the harvested RF energy from (1) can be written as

$$E_r' = \alpha\eta_1 \mathrm{tr}(\mathbf{H}\mathbf{P}_1\mathbf{H}^H) \tag{2}$$

where $\mathrm{tr}(\cdot)$ stands for the matrix trace and $0 < \eta_1 < 1$ is the efficiency of energy conversion at the EH unit[1]. It has been shown in [28]-[31] that the linear EH model (2) is optimistic, as in practice the harvested energy is bounded with the increase of the incident RF signal power. Moreover, practical EH circuits have limited harvesting sensitivity [32], i.e., the harvested power is zero when the input power is below the minimum power for harvesting. Considering both the upper-bound and limited sensitivity, we apply the constant-linear-constant (CLC) nonlinear EH model [32] in this paper

$$E_r = \begin{cases} 0, & \mathrm{tr}(\mathbf{H}\mathbf{P}_1\mathbf{H}^H) \le P_t; \\ \alpha E_m', & \eta_1 \mathrm{tr}(\mathbf{H}\mathbf{P}_1\mathbf{H}^H) \ge E_m'; \\ \alpha\eta_1 \mathrm{tr}(\mathbf{H}\mathbf{P}_1\mathbf{H}^H), & \text{otherwise.} \end{cases} \tag{3}$$

where P_t is the minimum input power for harvesting operation and E_m' is the maximum output power of the energy harvester.

During the second interval of βT, the source node transmits an $N_s \times 1$ information-carrying signal vector $\mathbf{s}_2$ to the relay node, where $0 < \beta < 1$ denotes the TS factor in the second interval and we assume that $E\{\mathbf{s}_2\mathbf{s}_2^H\} = \mathbf{P}_2$. The received information signal vector at the relay can be shown as

$$\mathbf{y}_{r,2} = \mathbf{H}\mathbf{s}_2 + \mathbf{v}_{r,2} \tag{4}$$

[1]Following [5], [27], the contribution of the noise component in (1) to the energy harvested at the relay node is negligible.

where $\mathbf{v}_{r,2}$ stands for the additive Gaussian noise during the second interval at the relay node with $E\{\mathbf{v}_{r,2}\mathbf{v}_{r,2}^H\} = \sigma_r^2\mathbf{I}_{N_r}$, where $\mathbf{I}_n$ denotes an $n \times n$ identity matrix. Then with the DF protocol, the relay node decodes the information from $\mathbf{y}_{r,2}$ and re-encodes it into an $N_r \times 1$ signal vector $\mathbf{x}_r$ with $E\{\mathbf{x}_r\mathbf{x}_r^H\} = \mathbf{Q}$.

In the third interval of γT, the relay node multicasts $\mathbf{x}_r$ to all L receivers, where $0 < \gamma < 1$ is the TS factor in the third interval. The received signal vector at the lth receiver can be written as

$$\mathbf{y}_{d,l} = \mathbf{G}_l\mathbf{x}_r + \mathbf{v}_{d,l}, \quad l = 1, \cdots, L \tag{5}$$

where $\mathbf{G}_l$ denotes an $N_d \times N_r$ MIMO channel matrix between the relay node and the lth receiver, and vector $\mathbf{v}_{d,l}$ denotes the additive Gaussian noise at the lth receiver with $E\{\mathbf{v}_{d,l}\mathbf{v}_{d,l}^H\} = \sigma_{d,l}^2\mathbf{I}_{N_d}$. Hereafter, we set $T = 1$ for the sake of notational simplicity. We would like to note that in the conventional TS protocol [19]-[23], the duration of both the second and the third intervals is set to $(1-\alpha)/2$, while in this paper, we introduce two new TS factors β and γ for the second interval and the third interval, respectively. It will be shown through simulations that this novel TS based protocol can achieve up to 60% higher system MI compared with the conventional TS protocol through a better time allocation between two hops of information transmission.

In this paper, we consider a typical EH based communication scenario where nodes in the system are either stationary or have a low mobility. In such scenario, all channels $\mathbf{G}_l, l = 1, \cdots, L$, and $\mathbf{H}$ are quasi-static and the required CSI can be estimated with a high precision, for example, through the methods in [39] and the references therein. The remaining very small mismatch between the true and the estimated CSI can be treated as noise as has been done in [23]. It is an interesting and challenging future topic to perform the overall system optimization taking into account the power/time required for channel acquisition. From (4) and (5), the system MI between the source node and all L receivers is given by

$$\mathrm{MI}(\beta,\gamma,\mathbf{P}_2,\mathbf{Q}) = \min\{\beta\log_2\left|\mathbf{I}_{N_r} + \sigma_r^{-2}\mathbf{H}\mathbf{P}_2\mathbf{H}^H\right|, \gamma\log_2|\mathbf{I}_{N_d}+\sigma_{d,1}^{-2}\mathbf{G}_1\mathbf{Q}\mathbf{G}_1^H|, \cdots, \gamma\log_2|\mathbf{I}_{N_d}+\sigma_{d,L}^{-2}\mathbf{G}_L\mathbf{Q}\mathbf{G}_L^H|\} \tag{6}$$

where $|\cdot|$ denotes the matrix determinant.

The energy used to transmit $\mathbf{s}_1$ and $\mathbf{s}_2$ at the source node is $\alpha\mathrm{tr}(\mathbf{P}_1)$ and $\beta\mathrm{tr}(\mathbf{P}_2)$, respectively. Thus, the energy consumption constraint at the source node is shown as

$$\alpha\mathrm{tr}(\mathbf{P}_1) + \beta\mathrm{tr}(\mathbf{P}_2) \le (\alpha+\beta)P_s \tag{7}$$

where P_s is the average source transmission power. Note that in [19], a constant power of information and energy transmission at the source node is assumed as

$$\mathrm{tr}(\mathbf{P}_1) \le P_s, \qquad \mathrm{tr}(\mathbf{P}_2) \le P_s. \tag{8}$$

In [21], the energy constraint at the source node is considered as

$$\alpha\mathrm{tr}(\mathbf{P}_1) + \frac{1-\alpha}{2}\mathrm{tr}(\mathbf{P}_2) \le \frac{1+\alpha}{2}P_s. \tag{9}$$

It can be noticed that (7) yields a larger feasible region than (8) and (9). In particular, (9) is a special case of (7) with $\beta = (1-\alpha)/2$. Moreover, when (8) is satisfied, (7) is also valid, but not vice versa. Thus, transceiver design may yield a better performance under the constraint of (7) than that of (8) and (9).

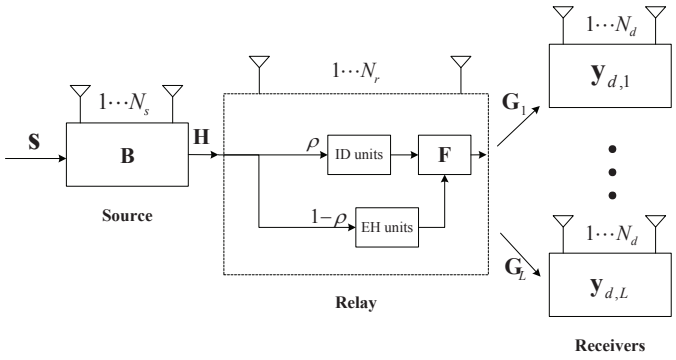

Fig. 3: Block diagram of the system with the PS based protocol.

At the relay node, the energy consumed to transmit $\mathbf{x}_r$ to the receivers during the third interval is given by

$$\gamma\mathrm{tr}(E\{\mathbf{x}_r\mathbf{x}_r^H\}) = \gamma\mathrm{tr}(\mathbf{Q}). \tag{10}$$

Following [33], we take into account the circuit energy consumption at the relay node, which includes two parts: A static part for the basic consumption of the circuit and a dynamic part that varies with the amount of information transmission. The static part is modeled as $\gamma N_r P_c$, where P_c denotes the static power consumption of each antenna [34]. The dynamic part is given by ξE_r, where $0 < \xi < 1$ [21]. From (3) and (10), the energy constraint at the relay node is shown as

$$\gamma(\mathrm{tr}(\mathbf{Q}) + N_r P_c) \le (1-\xi)E_r \tag{11}$$

From (6), (7), and (11), the problem of optimizing the MI in a DF multicasting MIMO relay system with a TS based EH relay node is given by

$$\max_{\mathbf{P}_1,\mathbf{P}_2,\mathbf{Q},\alpha,\beta,\gamma} \ \mathrm{MI}(\beta,\gamma,\mathbf{P}_2,\mathbf{Q}) \tag{12a}$$
$$\text{s.t. } \alpha\mathrm{tr}(\mathbf{P}_1) + \beta\mathrm{tr}(\mathbf{P}_2) \le (\alpha+\beta)P_s \tag{12b}$$
$$\gamma(\mathrm{tr}(\mathbf{Q}) + N_r P_c) \le (1-\xi)E_r \tag{12c}$$
$$0 < \alpha,\beta,\gamma < 1, \quad \alpha+\beta+\gamma \le 1 \tag{12d}$$
$$\mathbf{P}_1 \succeq 0, \quad \mathbf{P}_2 \succeq 0, \quad \mathbf{Q} \succeq 0. \tag{12e}$$

B. The PS Based Protocol

Fig. 3 shows that the total time $T = 1$ in the PS based protocol is equally divided into two time intervals. During the first interval, an $N_s \times 1$ information and energy-bearing signal vector $\mathbf{s}$ is transmitted to the relay node from the source node with $E\{\mathbf{s}\mathbf{s}^H\} = \mathbf{B}$. The received signal $\mathbf{y}_r$ at the relay node can be written as

$$\mathbf{y}_r = \mathbf{H}\mathbf{s} + \mathbf{v}_r \tag{13}$$

where $\mathbf{v}_r$ is the additive Gaussian noise vector at the relay node at the first interval with $E\{\mathbf{v}_r\mathbf{v}_r^H\} = \sigma_r^2\mathbf{I}_{N_r}$.

In the PS protocol, $\mathbf{y}_r$ is split into two parts for information transmission and EH at the relay node with a PS ratio of ρ, i.e.,

$(1-\rho)\mathbf{y}_r$ is applied for EH and $\rho\mathbf{y}_r$ is used for information transmission. Similar to (3), the harvested energy at the relay node with the PS based protocol can be shown as

$$E_{r,p}=\begin{cases}0, & \mathrm{tr}(\mathbf{HBH}^H)\le P_t;\\ \frac{1}{2}E'_m, & \eta_1(1-\rho)\mathrm{tr}(\mathbf{HBH}^H)\ge E'_m;\\ \frac{1}{2}\eta_1(1-\rho)\mathrm{tr}(\mathbf{HBH}^H), & \text{otherwise.}\end{cases} \tag{14}$$

In (3) and (14), a three-piecewise linear function is used to model the nonlinearity of EH, where before the minimal input power in reached, the output energy is zero, and after reaching saturation, the harvested energy remains stable, while in-between, the harvested energy increases linearly with the input power[2].

Meanwhile, the relay node decodes the information carried by $\rho\mathbf{y}_r$ and re-encodes it into an $N_r\times 1$ signal vector $\tilde{\mathbf{s}}$ with $E\{\tilde{\mathbf{s}}\tilde{\mathbf{s}}^H\}=\mathbf{R}$. During the second interval, $\tilde{\mathbf{s}}$ is multicast to L receivers. The received signal vector at the lth receiver is given by

$$\mathbf{y}_{d_l,p}=\mathbf{G}_l\tilde{\mathbf{s}}+\mathbf{v}_{d,l},\quad l=1,\cdots,L. \tag{15}$$

Based on (13) and (15), the MI between the source node and all L receivers with the PS protocol is given by

$$\mathrm{MI}(\rho,\mathbf{B},\mathbf{R})=\frac{1}{2}\min\{\log_2|\mathbf{I}_{N_r}+\rho\sigma_r^{-2}\mathbf{HBH}^H|,$$
$$\log_2|\mathbf{I}_{N_d}+\sigma_{d,1}^{-2}\mathbf{G}_1\mathbf{R}\mathbf{G}_1^H|,\cdots,\log_2|\mathbf{I}_{N_d}+\sigma_{d,L}^{-2}\mathbf{G}_L\mathbf{R}\mathbf{G}_L^H|\}. \tag{16}$$

At the source node, the energy consumption constraint can be written as

$$\mathrm{tr}(\mathbf{B})\le P_s. \tag{17}$$

The energy consumed to transmit $\tilde{\mathbf{s}}$ to the receivers during the second interval is $\frac{1}{2}\mathrm{tr}(\mathbf{R})$. By considering the circuit energy consumption, the energy constraint at the relay can be written as

$$\mathrm{tr}(\mathbf{R})+N_rP_c\le 2(1-\xi)E_{r,p}. \tag{18}$$

Then, from (16), (17), and (18), the optimal source and relay matrices design problem in DF multicasting MIMO relay systems with a PS based EH relay node is given by

$$\max_{\rho,\mathbf{B},\mathbf{R}}\ \mathrm{MI}(\rho,\mathbf{B},\mathbf{R}) \tag{19a}$$
$$\text{s.t. } \mathrm{tr}(\mathbf{B})\le P_s \tag{19b}$$
$$\mathrm{tr}(\mathbf{R})+N_rP_c\le 2(1-\xi)E_{r,p} \tag{19c}$$
$$\mathbf{B}\succeq 0,\quad \mathbf{R}\succeq 0,\quad 0<\rho<1. \tag{19d}$$

III. Proposed Transceiver Design Algorithms

A. TS Protocol with No Maximal Transmission Power Limits

The optimization problem (12) is challenging to solve because it is nonconvex with matrix variables. Compared with existing works such as [22] and [23], the challenges in solving the problem (12) are

- Three TS factors need to be optimized in the problem (12), while in [22] and [23], only a single TS factor is considered.
- The problem (12) is for a multicasting MIMO relay system with multiple receivers, while the systems in [22] and [23] have only a single receiver.
- A practical nonlinear EH model is considered in the problem (12), but not in [22] and [23].

In this section, an efficient algorithm for solving the problem (12) is proposed. First, the optimal structure of $\mathbf{P}_1$ and $\mathbf{P}_2$ is derived to simplify the problem (12). Let us introduce $\tilde{\mathbf{G}}_l=\sigma_{d,l}^{-1}\mathbf{G}_l$, $l=1,\cdots,L$ and the singular value decomposition (SVD) of $\mathbf{H}=\mathbf{U}_h\mathbf{\Lambda}_h^{\frac{1}{2}}\mathbf{V}_h^H$, where $\mathbf{\Lambda}_h=\mathrm{diag}(\lambda_{h,1},\cdots,\lambda_{h,R_h})$ with $\lambda_{h,1}\ge\lambda_{h,2}\ge\cdots\ge\lambda_{h,R_h}$, $R_h=\mathrm{rank}(\mathbf{H})$, $\mathrm{diag}(\cdot)$ means a diagonal matrix, and $\mathrm{rank}(\cdot)$ denotes the matrix rank.

Theorem 1: The optimal covariance matrices $\mathbf{P}_1$ and $\mathbf{P}_2$ have the following structure in terms of their eigenvalue decomposition (EVD) as the solution to the problem (12)

$$\mathbf{P}_1^*=\lambda_1\mathbf{v}_{h,1}\mathbf{v}_{h,1}^H,\quad \mathbf{P}_2^*=\mathbf{V}_h\mathbf{\Lambda}_2\mathbf{V}_h^H \tag{20}$$

where $(\cdot)^*$ denotes the optimal value, $\mathbf{\Lambda}_2$ is a $R_h\times R_h$ diagonal matrix, $\lambda_1>0$, and $\mathbf{v}_{h,1}$ is the first column of $\mathbf{V}_h$.

Proof: See Appendix A.

Interestingly, it can be observed from (20) that the optimal $\mathbf{P}_1$ matches $\mathbf{v}_{h,1}$, which means the maximum harvested energy can be achieved by beamforming at the source node to the strongest eigenmode of matrix $\mathbf{H}$. Consequently, there is $\mathrm{tr}(\mathbf{P}_1)=\lambda_1$ and the optimization of $\mathbf{P}_1$ is converted to the optimization of λ_1. We can also see from (20) that the optimal $\mathbf{P}_2$ matches $\mathbf{H}$. We would like to note that the structure of $\mathbf{P}_1$ in (20) was first derived in [5] for a one-hop SWIPT system, however, the optimization problem (12) is different to that in [5].

We can significantly simplify the problem (12) by substituting (20) back into (12). Firstly, the objective function (12a) can be written as

$$\mathrm{MI}(\beta,\gamma,\boldsymbol{\lambda}_2,\mathbf{Q})=\min\Big\{\beta\sum_{i=1}^{R_h}\log_2(1+\sigma_r^{-2}\lambda_{h,i}\lambda_{2,i}),$$
$$\gamma\log_2|\mathbf{I}_{N_d}+\tilde{\mathbf{G}}_1\mathbf{Q}\tilde{\mathbf{G}}_1^H|,\cdots,\gamma\log_2|\mathbf{I}_{N_d}+\tilde{\mathbf{G}}_L\mathbf{Q}\tilde{\mathbf{G}}_L^H|\}. \tag{21}$$

Then by using (21) and introducing an auxiliary variable t, which has the meaning of the system MI, the optimization problem (12) is rewritten as

$$\max_{\lambda_1,\boldsymbol{\lambda}_2,\mathbf{Q},t,\alpha,\beta,\gamma}\ t \tag{22a}$$
$$\text{s.t. } \beta\sum_{i=1}^{R_h}\log_2(1+\sigma_r^{-2}\lambda_{h,i}\lambda_{2,i})\ge t \tag{22b}$$
$$\gamma\log_2|\mathbf{I}_{N_d}+\tilde{\mathbf{G}}_l\mathbf{Q}\tilde{\mathbf{G}}_l^H|\ge t,\quad l=1,\cdots,L \tag{22c}$$
$$\alpha\lambda_1+\beta\sum_{i=1}^{R_h}\lambda_{2,i}\le(\alpha+\beta)P_s \tag{22d}$$
$$\gamma(\mathrm{tr}(\mathbf{Q})+N_rP_c)\le\alpha\eta\lambda_{h,1}\lambda_1 \tag{22e}$$
$$\gamma(\mathrm{tr}(\mathbf{Q})+N_rP_c)\le\alpha E_m \tag{22f}$$
$$\lambda_{h,1}\lambda_1\ge P_t \tag{22g}$$
$$0<\alpha,\beta,\gamma<1,\quad \alpha+\beta+\gamma\le 1 \tag{22h}$$
$$\mathbf{Q}\succeq 0,\qquad \lambda_{2,i}\ge 0,\ i=1,\cdots,R_h \tag{22i}$$

[2]It is shown in [32] that in practice the EH efficiency η_1 is a function of the input power. In this paper, similar to [19], [30], [31], we assume a constant η_1. Note that the algorithms proposed in this paper can be applied to any given η_1.

where $\eta = \eta_1(1-\xi)$, $E_m = (1-\xi)E'_m$, $\lambda_{2,i}$ stands for the ith diagonal element of $\mathbf{\Lambda}_2$ with $\boldsymbol{\lambda}_2 = [\lambda_{2,1}, \cdots, \lambda_{2,R_h}]^T$ and $(\cdot)^T$ denotes the matrix transpose.

By introducing $\tilde{\mathbf{Q}} = \gamma\mathbf{Q}$, $\tilde{\lambda}_1 = \alpha\lambda_1$, and $\tilde{\lambda}_{2,i} = \beta\lambda_{2,i}$, $i = 1, \cdots, R_h$, (22) is recast as

$$\max_{\tilde{\lambda}_1, \tilde{\boldsymbol{\lambda}}_2, \tilde{\mathbf{Q}}, t, \alpha, \beta, \gamma} \quad t \tag{23a}$$

$$\text{s.t. } \beta \sum_{i=1}^{R_h} \log_2(1 + \sigma_r^{-2}\lambda_{h,i}\tilde{\lambda}_{2,i}/\beta) \geq t \tag{23b}$$

$$\gamma \log_2|\mathbf{I}_{N_d} + \tilde{\mathbf{G}}_l\tilde{\mathbf{Q}}\tilde{\mathbf{G}}_l^H/\gamma| \geq t, \quad l = 1, \cdots, L \tag{23c}$$

$$\tilde{\lambda}_1 + \sum_{i=1}^{R_h} \tilde{\lambda}_{2,i} \leq (\alpha+\beta)P_s \tag{23d}$$

$$\mathrm{tr}(\tilde{\mathbf{Q}}) + \gamma N_r P_c \leq \eta\lambda_{h,1}\tilde{\lambda}_1 \tag{23e}$$

$$\mathrm{tr}(\tilde{\mathbf{Q}}) + \gamma N_r P_c \leq \alpha E_m \tag{23f}$$

$$\lambda_{h,1}\tilde{\lambda}_1 \geq \alpha P_t \tag{23g}$$

$$0 < \alpha, \beta, \gamma < 1, \ \alpha + \beta + \gamma < 1 \tag{23h}$$

$$\tilde{\mathbf{Q}} \succeq 0, \qquad \tilde{\lambda}_{2,i} \geq 0, \ i = 1, \cdots, R_h \tag{23i}$$

where $\tilde{\boldsymbol{\lambda}}_2 = [\tilde{\lambda}_{2,1}, \cdots, \tilde{\lambda}_{2,R_h}]^T$. Since $\log_2(1 + \sigma_r^{-2}\lambda_{h,i}\tilde{\lambda}_{2,i})$ and $\log_2|\mathbf{I}_{N_d} + \tilde{\mathbf{G}}_l\tilde{\mathbf{Q}}\tilde{\mathbf{G}}_l^H|$ are concave functions of $\tilde{\lambda}_{2,i}$ and $\tilde{\mathbf{Q}}$, respectively. Based on the concept of the perspective function in Section 3.2.6 of [37], $\beta\log_2(1+\sigma_r^{-2}\lambda_{h,i}\tilde{\lambda}_{2,i}/\beta)$ is concave with respect to $(\beta, \tilde{\lambda}_{2,i})$ and $\gamma\log_2|\mathbf{I}_{N_d} + \tilde{\mathbf{G}}_l\tilde{\mathbf{Q}}\tilde{\mathbf{G}}_l^H/\gamma|$ is a concave function of $(\gamma, \tilde{\mathbf{Q}})$. Thus, we can see that (23b) and (23c) are convex constraints. It can be easily seen that (23d)-(23i) are convex constraints. Therefore, the problem (23) is a jointly convex problem in the design parameters. In particular, the problem (23) is a nonlinear semidefinite programming (SDP) problem, which can be solved efficiently through the CVX toolbox [38] for disciplined convex programming.

The procedure of the TS based transceiver design with no maximal transmission power limits is summarized in Algorithm 1. Since the source node has a stable power supply, Algorithm 1 is best to be run at the source node with the CSI of $\mathbf{H}$ and $\mathbf{G}_l, l = 1, \cdots, L$. Then the source node sends the optimal $\mathbf{Q}$ to the relay node. Since the problem (23) is convex, The proposed Algorithm 1 achieves the global optimum of the problem (12).

Algorithm 1 Proposed Transceiver Optimization Algorithm Based on the Novel TS Protocol without Maximal Transmission Power Limits

Input: P_s, E_m, $\mathbf{H}$, σ_r^2, $\mathbf{G}_l$, $\sigma_{d,l}^2$, $l = 1, \cdots, L$.
Output: α^*, β^*, γ^*, $\mathbf{P}_1^*$, $\mathbf{P}_2^*$, and $\mathbf{Q}^*$.
1: Calculate $\tilde{\mathbf{G}}_l = \sigma_{d,l}^{-1}\mathbf{G}_l$, $l = 1, \cdots, L$.
2: Calculate the SVD of $\mathbf{H}$.
3: Solve the problem (23) to obtain $\tilde{\lambda}_1^*$, $\tilde{\boldsymbol{\lambda}}_2^*$, $\tilde{\mathbf{Q}}^*$, α^*, β^*, γ^*.
4: Calculate $\mathbf{Q}^* = \tilde{\mathbf{Q}}^*/\gamma^*$, $\lambda_1^* = \tilde{\lambda}_1^*/\alpha^*$, and $\lambda_{2,i}^* = \tilde{\lambda}_{2,i}^*/\beta^*$, $i = 1, \cdots, R_h$.
5: Obtain $\mathbf{P}_1^*$ and $\mathbf{P}_2^*$ by (20).

B. TS Protocol with Maximal Transmission Power Limits

It can be seen from the problem (12) that the transmission power of the source and relay may approach a very large value when the TS factors α, β, or γ approach 0. For example, when β is close to 0, a very large $\mathbf{P}_2$ would still make the constraint (12b) valid. Similarly, from (12c) we can see that if γ approaches 0, the transmission power of the relay node $\mathrm{tr}(\mathbf{Q})$ may approach a very large value without violating (12c). Thus, for practical relay systems, we need to consider maximal transmission power limits at the source node and the relay node as

$$\mathrm{tr}(\mathbf{P}_1) \leq P_{m,s}, \quad \mathrm{tr}(\mathbf{P}_2) \leq P_{m,s}, \quad \mathrm{tr}(\mathbf{Q}) \leq P_{m,r} \tag{24}$$

where $P_{m,s}$ and $P_{m,r}$ are the peak transmission power at the source and relay nodes, respectively. Based on (20), the peak power constraints in (24) can be recast as

$$\lambda_1 \leq P_{m,s}, \quad \sum_{i=1}^{R_h} \lambda_{2,i} \leq P_{m,s}, \quad \mathrm{tr}(\mathbf{Q}) \leq P_{m,r}. \tag{25}$$

By incorporating (25) into the problem (23), the TS protocol based transceiver optimization problem with peak power constraints is given by

$$\max_{\tilde{\lambda}_1, \tilde{\boldsymbol{\lambda}}_2, \tilde{\mathbf{Q}}, t, \alpha, \beta, \gamma} \quad t \tag{26a}$$

$$\text{s.t. } \beta \sum_{i=1}^{R_h} \log_2(1 + \sigma_r^{-2}\lambda_{h,i}\tilde{\lambda}_{2,i}/\beta) \geq t \tag{26b}$$

$$\gamma \log_2|\mathbf{I}_{N_d} + \tilde{\mathbf{G}}_l\tilde{\mathbf{Q}}\tilde{\mathbf{G}}_l^H/\gamma| \geq t, \quad l = 1, \cdots, L \tag{26c}$$

$$\tilde{\lambda}_1 + \sum_{i=1}^{R_h} \tilde{\lambda}_{2,i} \leq (\alpha+\beta)P_s \tag{26d}$$

$$\mathrm{tr}(\tilde{\mathbf{Q}}) + \gamma N_r P_c \leq \eta\lambda_{h,1}\tilde{\lambda}_1 \tag{26e}$$

$$\mathrm{tr}(\tilde{\mathbf{Q}}) + \gamma N_r P_c \leq \alpha E_m \tag{26f}$$

$$\sum_{i=1}^{R_h} \tilde{\lambda}_{2,i} \leq \beta P_{m,s}, \quad \mathrm{tr}(\tilde{\mathbf{Q}}) \leq \gamma P_{m,r} \tag{26g}$$

$$0 < \alpha, \beta, \gamma < 1, \ \alpha + \beta + \gamma < 1, \ \tilde{\mathbf{Q}} \succeq 0 \tag{26h}$$

$$\frac{\alpha P_t}{\lambda_{h,1}} \leq \tilde{\lambda}_1 \leq \alpha P_{m,s}, \tilde{\lambda}_{2,i} \geq 0, \quad i = 1, \cdots, R_h. \tag{26i}$$

The peak power constraints in (26g) and (26i) are convex. Thus, the optimization problem (26) is a convex nonlinear SDP problem and can be easily solved at the source node by the CVX toolbox [38], and the optimal $\mathbf{Q}$ is sent to the relay node from the source node. The procedure of the TS based transceiver optimization with maximal transmission power limits is similar to Algorithm 1, except that the third step of Algorithm 1 is replaced by solving the problem (26), and the value of $P_{m,s}$ and $P_{m,r}$ is required as additional input. Since the problem (26) is convex, the proposed solution achieves the global optimum.

C. PS Based Protocol

In this subsection, an efficient algorithm for solving the optimization problem (19) is proposed to obtain the maximal system MI for the PS based protocol.

Theorem 2: The optimal covariance matrix $\mathbf{B}$ as the solution to the problem (19) is given by

$$\mathbf{B}^* = \mathbf{V}_h\mathbf{\Lambda}_b\mathbf{V}_h^H \tag{27}$$

where $\mathbf{\Lambda}_b$ is a $R_h \times R_h$ diagonal matrix.

Proof: See Appendix B.

By substituting (27) into (19), the problem (19) can be recast as a simpler optimization problem

$$\max_{\rho,\boldsymbol{\lambda}_b,\mathbf{R},t} \quad \frac{t}{2} \tag{28a}$$

$$\text{s.t.} \sum_{i=1}^{R_h} \log_2(1+\sigma_r^{-2}\lambda_{h,i}\lambda_{b,i}\rho) \geq t \tag{28b}$$

$$\log_2|\mathbf{I}_{N_d}+\tilde{\mathbf{G}}_l\mathbf{R}\tilde{\mathbf{G}}_l^H| \geq t, \quad l=1,\cdots,L \tag{28c}$$

$$\sum_{i=1}^{R_h} \lambda_{b,i} \leq P_s \tag{28d}$$

$$\sum_{i=1}^{R_h} \lambda_{h,i}\lambda_{b,i} \geq P_t \tag{28e}$$

$$\text{tr}(\mathbf{R}) \leq \sum_{i=1}^{R_h} \eta(1-\rho)\lambda_{h,i}\lambda_{b,i} - N_rP_c \tag{28f}$$

$$\text{tr}(\mathbf{R}) \leq E_m - N_rP_c \tag{28g}$$

$$0<\rho<1, \ \ \mathbf{R}\succeq 0, \ \ \lambda_{b,i}\geq 0, \ i=1,\cdots,R_h \tag{28h}$$

where $\lambda_{b,i}$ denotes the ith diagonal element of $\mathbf{\Lambda}_b$ with $\boldsymbol{\lambda}_b=[\lambda_{b,1},\cdots,\lambda_{b,R_h}]^T$. Considering the path loss, we have $\lambda_{h,i}<1$. Thus, we have $\sum_{i=1}^{R_h}\eta(1-\rho)\lambda_{h,i}\lambda_{b,i}-N_rP_c<\sum_{i=1}^{R_h}\lambda_{b,i}\leq P_s$. Thus, for the PS based protocol, there is no need to introduce peak transmission power constraints. For a given ρ, the problem (28) becomes

$$\max_{\boldsymbol{\lambda}_b,\mathbf{R},t} \quad \frac{t}{2} \tag{29a}$$

$$\text{s.t.} \sum_{i=1}^{R_h} \log_2(1+\sigma_r^{-2}\lambda_{h,i}\lambda_{b,i}\rho) \geq t \tag{29b}$$

$$\log_2|\mathbf{I}_{N_d}+\tilde{\mathbf{G}}_l\mathbf{R}\tilde{\mathbf{G}}_l^H| \geq t, \quad l=1,\cdots,L \tag{29c}$$

$$\sum_{i=1}^{R_h} \lambda_{b,i} \leq P_s \tag{29d}$$

$$\sum_{i=1}^{R_h} \lambda_{h,i}\lambda_{b,i} \geq P_t \tag{29e}$$

$$\text{tr}(\mathbf{R}) \leq \sum_{i=1}^{R_h} \eta(1-\rho)\lambda_{h,i}\lambda_{b,i} - N_rP_c \tag{29f}$$

$$\text{tr}(\mathbf{R}) \leq E_m - N_rP_c \tag{29g}$$

$$\mathbf{R}\succeq 0, \ \ \lambda_{b,i}\geq 0, \ i=1,\cdots,R_h. \tag{29h}$$

The optimization problem (29) is a jointly convex nonlinear SDP problem. Therefore, the problem (28) can be solved through a golden section search in $(0,1)$ for the optimal ρ, where in each search step, the CVX toolbox [38] is used to solve the problem (29) for the optimal $\boldsymbol{\lambda}_b, \mathbf{R}, t$. The procedure of the PS based transceiver design is listed in Algorithm 2, where ε is a positive constant close to 0 and $\delta=1.618$ is the golden ratio. Similar to Algorithm 1, Algorithm 2 is solved at the source node and the optimal ρ and $\mathbf{Q}$ are sent to the relay node by the source node. However, since the transceiver optimization problem (28) is not jointly convex in all design parameters, we cannot prove that Algorithm 2 achieves the global optimum of the problem (28).

Algorithm 2 Proposed Transceiver Optimization Algorithm Based on the PS Protocol

Input: P_s, E_m, $\mathbf{H}$, σ_r^2, $\mathbf{G}_l$, $\sigma_{d,l}^2$, $l=1,\cdots,L$.
Output: ρ^*, $\mathbf{B}^*$, and $\mathbf{R}^*$.
1: Calculate $\tilde{\mathbf{G}}_l=\sigma_{d,l}^{-1}\mathbf{G}_l$, $l=1,\cdots,L$.
2: Calculate the SVD of $\mathbf{H}$.
Initialization: $\rho_l=0$ and $\rho_u=1$.
3: **while** $\rho_u-\rho_l>\varepsilon$ **do**
4: Define $\rho_1=(\delta-1)\rho_l+(2-\delta)\rho_u$ and $\rho_2=(2-\delta)\rho_l+(\delta-1)\rho_u$.
5: Solve the problem (29) with ρ_1, whose solution is denoted as $\boldsymbol{\lambda}_{b,1}$, $\mathbf{R}_1$, and t_1.
6: Solve the problem (29) with ρ_2 to obtain the solution as $\boldsymbol{\lambda}_{b,2}$, $\mathbf{R}_2$, and t_2.
7: **if** $t_1<t_2$ **then**
8: Assign $\rho_l=\rho_1$.
9: **else**
10: Assign $\rho_u=\rho_2$.
11: **end if**
12: **end while**
13: Calculate $\mathbf{R}^*=(\mathbf{R}_1+\mathbf{R}_2)/2$ and $\boldsymbol{\lambda}_b^*=(\boldsymbol{\lambda}_{b,1}+\boldsymbol{\lambda}_{b,2})/2$.
14: Obtain $\mathbf{B}^*$ according to (27).

Remark: For both the TS and PS based protocols, the proposed approaches are the first algorithms which provide the transceiver design for DF multicasting MIMO relay systems with an EH relay node following the practical nonlinear EH model by considering both the upper-bound and limited sensitivity of the EH circuit.

D. Computational Complexity of the Proposed Algorithms

In this subsection, we present the computational complexity analysis of the proposed algorithms. For the TS protocol with no maximal transmission power limits, the problem (23) is a nonlinear convex SDP problem. How to efficiently solve this type of problems is an active research area [40]. In general, the computational complexity of solving nonlinear convex SDP problem is higher than that of the linear convex SDP problem. It is shown in [40, Theorem 8.3] that the complexity order of solving a nonlinear convex SDP problem by the augmented Lagrangian method is $\mathcal{O}(m^3n+m^2n^2+n^3)$, where n is the dimension of the optimization variables and m is the dimension of the $m\times m$ semidefinite constraint. Based on this, the problem (23) can be solved at a complexity order of $\mathcal{O}(m_1^3n_1+m_1^2n_1^2+n_1^3)$, where $m_1=N_r+R_h+L+12$ and $n_1=N_r^2+R_h+5$.

For the TS protocol with maximal transmission power limits, using a similar analysis, the computational complexity order of solving the problem (26) is given by $\mathcal{O}(m_2^3n_1+m_2^2n_1^2+n_1^3)$, where $m_2=N_r+R_h+L+15$. Apparently, due to the additional peak power constraints in (26g) and (26i), the complexity of solving the problem (26) is higher than that of the problem (23).

Regarding the PS based protocol, the complexity order of solving the problem (28) is given by $\mathcal{O}(c(m_3^3n_2+m_3^2n_2^2+n_2^3))$, where $m_3=N_r+R_h+L+5$, $n_2=N_r^2+R_h+1$, and c denotes the number of golden section trials in finding the optimal ρ.

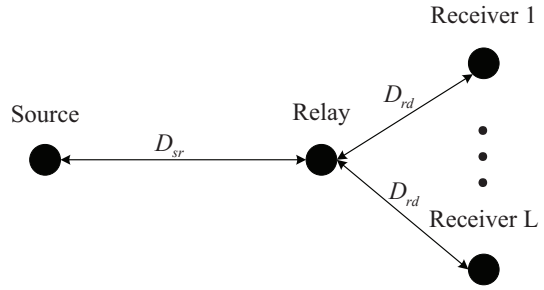

Fig. 4: The placement of the source, relay, and receivers.

We can see that for small N_r, R_h, L, and c, the complexity order of solving the problem (28) is lower than that of the problem (26) and the problem (23). For systems with large N_r, R_h, and L, the computational complexity order of the PS based protocol can be higher than that of the TS based protocol.

IV. Simulation Results

In this section, numerical simulation results for the proposed algorithms are presented. We consider a case where the source node, the relay node, and L receivers are placed as shown in Fig. 4. For the simplicity of notations, the receivers are assumed to be placed with equal distance to the relay node. Without specifically mentioned, $D_{sr} = 10d$ meters and $D_{rd} = 10(2-d)$ meters stand for the distances of source to relay, and relay to receivers, respectively. Note that as reported in [41], this is a typical distance of RF-based wireless power transfer. We normalize the value of $0 < d < 2$ over 10 meters, which makes it easier to determine if the relay node is closer to the receivers ($1 < d < 2$) or nearer to the source node ($0 < d < 1$). Except for the last numerical example, the channel matrices are modeled as $\mathbf{H} = D_{sr}^{-\varsigma/2}\bar{\mathbf{H}}$ and $\mathbf{G}_l = D_{rd}^{-\varsigma/2}\bar{\mathbf{G}}_l$, $l = 1, \cdots, L$, where $\bar{\mathbf{H}}$ and $\bar{\mathbf{G}}_l$ are the small-scale Rayleigh fading, $D_{sr}^{-\varsigma}$ and $D_{rd}^{-\varsigma}$ stand for the large-scale path loss, and ς represents the path loss exponent. Here $\varsigma = 3$ is chosen in the simulations. For the small-scale Rayleigh fading, $\bar{\mathbf{H}}$ and $\bar{\mathbf{G}}_l$ have i.i.d. complex Gaussian elements with zero mean and variances of $1/N_s$ and $1/N_r$, respectively.

For all numerical examples, we set the number of antennas $N_s = N_r = N_d = N$, the minimum input power for harvesting $P_t = -35$ dBm, and the static power consumption at each antenna of the relay node as $P_c = 1\mu$W. Unless mentioned otherwise, we choose the efficiency as $\eta = 0.7$, and the noise variance at the relay node and each receiver as $\sigma_r^2 = \sigma_{d,l}^2 = -50$ dBm, $l = 1, \cdots, L$. For the TS based protocol with source and relay nodes peak power constraints, we choose $P_{m,s} = P_{m,r} = KP_s$ ($K \geq 1$). All simulation results are obtained by averaging over 500 independent realizations of $\mathbf{H}$ and $\mathbf{G}_l$.

A. Example 1: Energy Constraint versus Source Node Power

We first study the power constraint at the relay node by checking the right-hand side of (11) and (18). We choose $N = 3$, $d = 1$, and $L = 2$. Fig. 5 demonstrates the right-hand side of (11) in the TS protocol without maximal transmission power limits versus the average source node power P_s at various E_m. From Fig. 5, we can observe that the ideal linear EH model (without any E_m limit) provides an upper-bound of the energy harvested at the relay node. For the practical nonlinear EH model (3), the harvested energy is not affected by E_m at low P_s, as the EH circuit is in its linear range when the input power is low. The effect of E_m can be clearly seen at medium and high P_s as the curves bend downwards and eventually remain flat. We can also observe from Fig. 5 that as E_m decreases, the available energy at the relay node reduces and the "turning point" where a curve starts bending downwards appears at a lower P_s. We choose $E_m = 0.25$ mW in the following simulation examples.

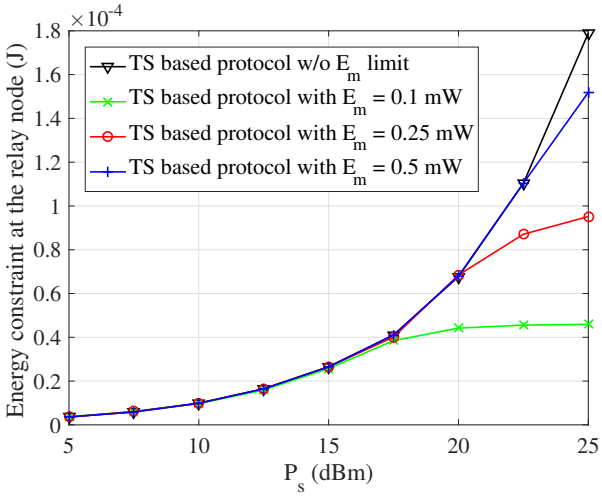

Fig. 5: Example 1: Energy constraint of the relay node in the TS protocol versus the average source node power; $N = 3$, $d = 1$, and $L = 2$.

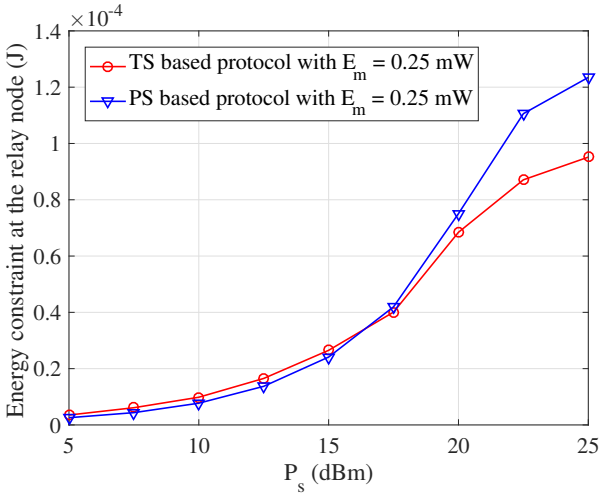

Fig. 6: Example 1: Energy constraint at the relay node in the TS and PS protocols versus the average source node power; $N = 3$, $d = 1$, and $L = 2$.

Fig. 6 shows the right-hand side of (11) in the TS protocol with no maximal transmission power limits and the right-hand side of (18) in the PS protocol versus P_s at $E_m = 0.25$ mW.

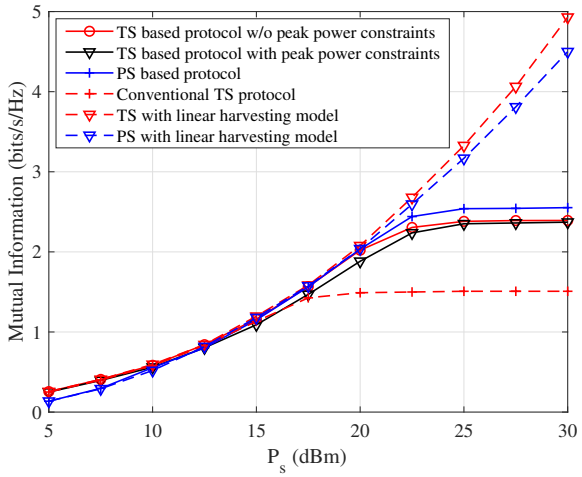

Fig. 7: Example 2: MI versus P_s; $N = 3$, $d = 1$, $L = 2$, and $K = 1$.

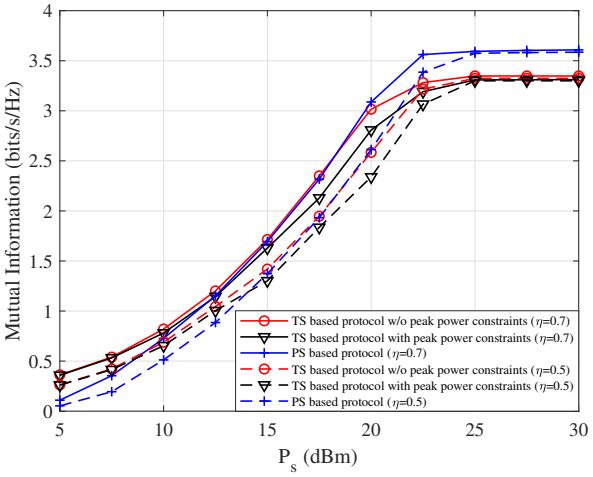

Fig. 8: Example 2: MI versus P_s; $N = 5$, $d = 1$, $L = 2$, and $K = 1$.

Interestingly, we can see from Fig. 6 that for the TS protocol, the available energy at the relay node is higher at low and medium P_s where the bound E_m is not reached. At high P_s where the bound E_m is active, the PS based protocol has a higher harvested energy. This is because when the EH bound E_m is approached at high P_s, from (22f) the energy harvested by the TS based protocol is αE_m and the energy harvested by the PS based protocol according to (28g) is $0.5E_m$. From the optimal solution of α shown in Fig. 13, we find that $\alpha = 0.37 < 0.5$ for large P_s.

B. Example 2: MI versus the Average Source Node Power

In the second example, we set $d = 1$, $L = 2$, and $K = 1$. Fig. 7 and Fig. 8 show the achievable MI of multicasting systems using the three protocols versus the average source node transmission power P_s with $N = 3$ and $N = 5$, respectively. As benchmarks, the MI of the following three baseline schemes is also shown in Fig. 7:

- Conventional TS based protocol [22], [23] with a single TS factor, using (9) as the energy constraint, and adopting the nonlinear EH model (3).
- The proposed TS protocol but with the conventional linear EH model.
- The PS protocol with the linear EH model.

It can be seen from Fig. 7 that compared with the existing TS protocol, the proposed TS based protocol can achieve a higher system MI. In particular, when the harvested energy bound is reached when $P_s > 22.5$ dBm, the performance of the proposed TS protocol greatly exceeds the existing TS protocol (with 60% higher MI at $P_s = 25$ dBm). The reason is two fold. Firstly, we note that in the conventional TS based protocol, the system MI is given by

$$\mathrm{MI}(\alpha, \mathbf{P}_2, \mathbf{Q}) = \frac{1-\alpha}{2} \min\{\log_2 \left|\mathbf{I}_{N_r} + \sigma_r^{-2}\mathbf{H}\mathbf{P}_2\mathbf{H}^H\right|, \log_2|\mathbf{I}_{N_d}+\sigma_{d,1}^{-2}\mathbf{G}_1\mathbf{Q}\mathbf{G}_1^H|, \cdots, \log_2|\mathbf{I}_{N_d}+\sigma_{d,L}^{-2}\mathbf{G}_L\mathbf{Q}\mathbf{G}_L^H|\}. \quad (30)$$

It can be seen that compared with a single TS factor $\frac{1-\alpha}{2}$ in (30), the two TS factors β and γ in (6) enable the balance between the MI of the source-relay link and the MI of the relay-receivers links, and thus, the optimal value of (6) is larger than that of (30). Secondly, the introduction of β and γ makes the saturation of the EH circuit at $P_s = 22.5$ dBm, while with only a single TS factor the EH circuit gets saturated at $P_s = 17.5$ dBm. Furthermore, for the linear EH model, Fig. 7 illustrates the system MI of both the TS based and PS based protocols increases with the increase of the source energy[3], and the TS based protocol outperforms that of the PS based protocol, since the energy harvested by the TS protocol is larger under the linear EH model (see Fig. 6 and the explanations before).

In Fig. 8, the achievable system MI is shown with $\eta = 0.7$ and $\eta = 0.5$. It can be seen that for all three protocols, the system MI decreases when η is reduced from 0.7 to 0.5. Since $\eta = \eta_1(1-\xi)$ and the dynamic part of the circuit energy consumption at the relay node is modeled as ξE_r, Fig. 8 shows that for both the TS and PS protocols, the achievable MI decreases with the relay node circuit energy consumption.

Considering the practical nonlinear EH model, from Figs. 7 and 8, it can be observed that the system MI saturates for $P_s > 25$ dBm. At low P_s, the TS protocol has a larger system MI compared with the PS protocol as the former one harvests more energy (see Fig. 6). The TS protocol with strict maximal transmission power limits ($K = 1$) has a lower system MI compared with the PS based protocol at medium and high P_s. Moreover, it also can be observed that the TS protocol with no maximal transmission power limits yields a higher system MI than that with maximal transmission power limits. This is due to the latter protocol has a smaller feasible region than the former one.

Interestingly, it also can be seen that the proposed novel TS protocol with no maximal transmission power limits outperforms the PS based protocol when the harvested power does

[3]One way to extend the linear region of the EH receiver, and thus increase the system MI, is to to have a separate EH circuit for each antenna at the relay node, instead of having only a single EH circuit for the entire relay node.

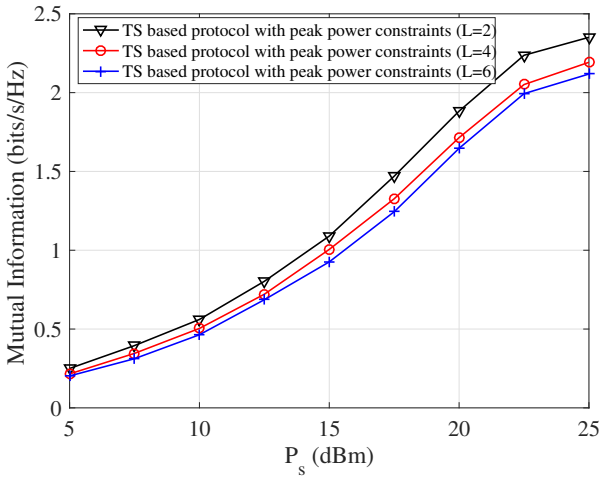

Fig. 9: Example 3: MI of the TS protocol versus P_s with various number of receivers; $N = 3$, $d = 1$, and $K = 1$.

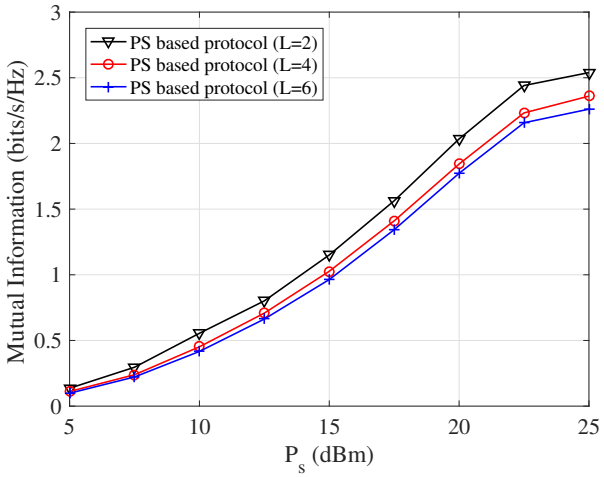

Fig. 10: Example 3: MI of the PS protocol versus P_s with various number of receivers; $N = 3$ and $d = 1$.

not approach the bound E_m (at low and medium P_s). However, when E_m is approached (at high P_s), the PS protocol has a larger MI. The reason can be explained below. When the bound E_m is reached, the energy constraints (22f) and (28g) become tight, which can be written as $\mathrm{tr}(\mathbf{Q}) + N_r P_c = \frac{\alpha}{\gamma} E_m$ and $\mathrm{tr}(\mathbf{R}) + N_r P_c = E_m$ for the TS and PS protocols, respectively. From the optimal solution of α and γ shown in Figs. 13 and 14 later on, we find that $\alpha/\gamma = 0.37/0.53 = 0.7$ for large P_s. Thus, the transmission power available for the TS based protocol is lower than that for the PS based protocol when the bound E_m is approached.

By comparing Fig. 7 with Fig. 8, it can be seen that for all the three protocols studied, the system MI increases with the number of antennas, which indicates the benefits of the MIMO technology. The simulation results in Figs. 7 and 8 provide useful guidance in selecting P_s to achieve a given data rate under certain system configurations.

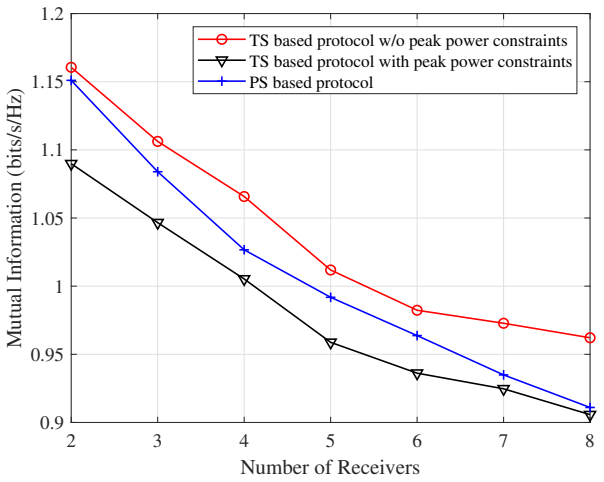

Fig. 11: Example 3: MI versus the number of receivers; $N = 3$, $d = 1$, and $P_s = 15$ dBm.

C. Example 3: System MI with Various Number of Receivers

In the next simulation example, we set $N = 3$, $d = 1$, and $K = 1$. The system MI of the TS and PS protocols versus the average source node transmission power P_s with the number of receivers at $L = 2$, $L = 4$, and $L = 6$ is shown in Fig. 9 and Fig. 10. In addition, Fig. 11 shows the system MI versus the number of receivers at $P_s = 15$ dBm. From these three figures, it can be seen that the system MI decreases as the number of receivers increases. This phenomenon has also been observed in [36], where it has been proven that with the number of receivers L approaches infinity, the multicasting rate converges to zero. The reason for the decrease of the MI with increasing number of users in a multicasting system is due to the nature of channel, since the multicasting rate is governed by the weakest channel among all users. Statistically, the weakest channel among a larger number of users is worse than that among a smaller number of users. Note that in realistic multicasting scenarios, the number of users is usually limited, and thus, a nonzero multicasting rate is achievable.

D. Example 4: TS Protocol with Various Maximal Transmission Power Limits

In the fourth example, we set $N = 3$, $d = 1$, and $L = 2$. Fig. 12 shows the MI of the TS protocol versus the average source node power P_s with maximal transmission power limits at $K = 1$ and $K = 10$. We can see from Fig. 12 that the system MI of the TS protocol with maximal transmission power limits increases with the increment of the power constraints $P_{m,s}$ and $P_{m,r}$. Moreover, the system MI is almost the same as that of the TS protocol with no maximal transmission power limits when $P_{m,s}$ and $P_{m,r}$ are large enough ($K = 10$). The reason is that when the power limits are high, the peak power constraints in (26g) and (26i) are easily satisfied.

E. Example 5: Optimal TS Factors of the TS Based Protocol

In this numerical example, we set $N = 3$, $d = 1$, $L = 2$, and show the optimal value of the TS factors α and γ in the TS

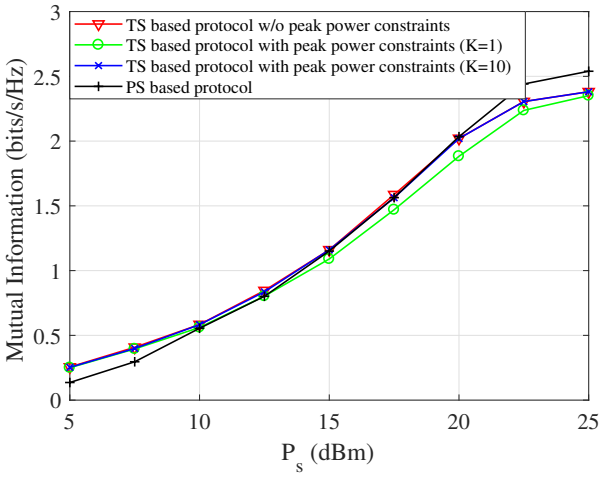

Fig. 12: Example 4: MI of the TS protocol versus P_s with various peak power constraints; $N = 3$, $d = 1$, and $L = 2$.

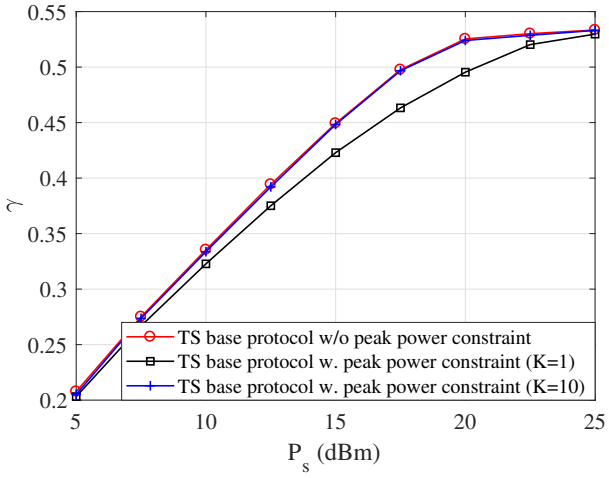

Fig. 14: Example 5: TS factor γ versus P_s; $N = 3$, $d = 1$, and $L = 2$.

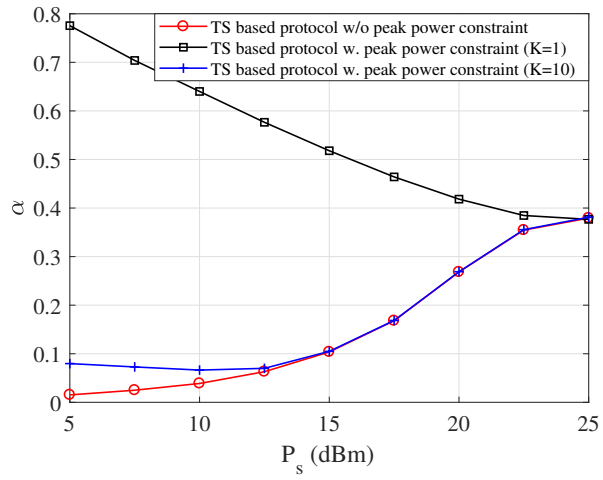

Fig. 13: Example 5: TS factor α versus P_s; $N = 3$, $d = 1$, and $L = 2$.

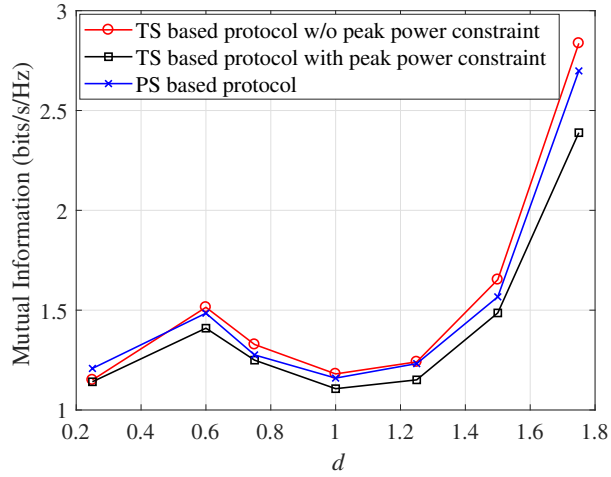

Fig. 15: Example 6: MI versus d; $N = 3$, $L = 2$, $K = 1$, and $P_s = 15$ dBm.

based protocol (with and without maximal transmission power limits) versus the average source node power P_s in Figs. 13 and 14. It can be seen that the optimal value of α increases as the source node power P_s increases for the TS based protocol with no maximal transmission power limits. Note that it has been shown in [22] that for an ideal linear EH relay node without any E_m limit, the optimal α decreases with P_s and approaches zero at high P_s. This is because in the absence of the E_m limit, even a small α enables the relay node to harvest enough energy at the first interval, due to the energy constraint (7), which is also the reason of a small α at low P_s in Fig. 13. However, based on the nonlinear EH model (3), as the harvested power is limited by E_m (see (23f)), α needs to increase as P_s increases to optimize the system MI.

For the TS protocol with maximal transmission power limits, the trend of the optimal α is nearly the same as that without peak power constraints when $K = 10$. For $K = 1$, the optimal α is larger than that with no maximal transmission power limits. This is because under the strict peak power constraint (26i), α must be large enough so that the relay node can harvest enough energy for information transmission in the last time interval. Moreover, in this case, the optimal α decreases as P_s increases, as a shorter time is needed to harvest enough energy as P_s increases.

Interestingly, it can be observed from Fig. 14 that the optimal γ increases with the increment of P_s and the value of the maximal transmission power limits K. The TS based protocol without maximal transmission power limits has the largest γ among the three systems.

F. Example 6: Achievable MI at Various Locations of the Relay Node

In this numerical example, we set $N = 3$, $L = 2$, $K = 1$, and plot the achievable MI versus d for the three protocols with $P_s = 15$ dBm and $P_s = 25$ dBm in Fig. 15 and Fig. 16, respectively. Fig. 15 presents that for $P_s = 15$ dBm and all

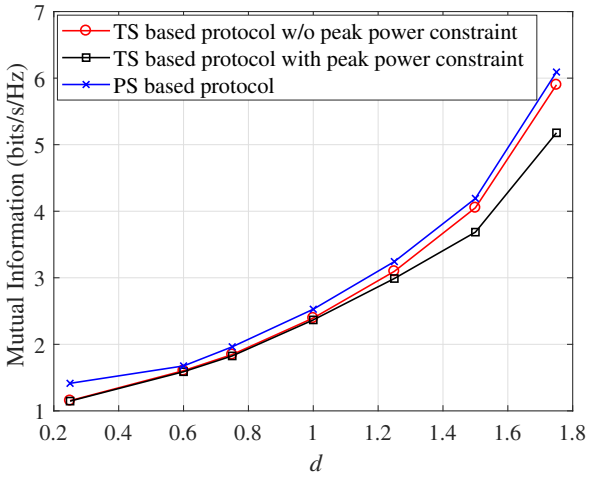

Fig. 16: Example 6: MI versus d; $N = 3$, $L = 2$, $K = 1$, and $P_s = 25$ dBm.

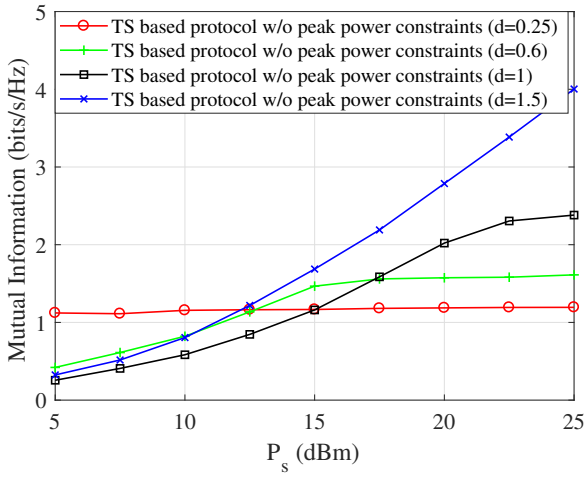

Fig. 17: Example 6: MI of the TS based protocol without peak power constraints versus P_s at various d; $N = 3$ and $L = 2$.

$d < 0.6$, the harvested power approaches the bound E_m even at a medium P_s, due to the short source-relay distance. This indicates that for $d < 0.6$, placing the relay node closer to the source node (i.e., reducing d) does not help the relay node to harvest more energy, while the second-hop channel is stronger at $d = 0.6$ than $d = 0.25$. Thus, for all three protocols, the system MI is lower at $d = 0.25$ than that at $d = 0.6$. When $d \geq 0.6$, the EH circuit works in the linear range and the bound E_m is not reached. In this case, we can observe from Fig. 15 that for all three protocols, the achievable MI decreases first and then increases with the increase of d. And the minimum value is obtained when $d = 1$, where the relay node is located at the midpoint between the source node and the receivers. The reason can be explained below. When the relay node is located closer to the source node ($0.6 < d < 1$), the relay node can harvest more energy from the source node which leads to a higher MI with the decrease of d. When the relay node is closer to the receivers ($1 < d < 2$), although the relay node harvests less energy from the source node, the achievable system MI can also increase due to a stronger relay-receiver channel.

When $P_s = 25$ dBm, the harvested power at the relay node approaches the bound E_m at all distances ($0 < d < 2$). We can observe from Fig. 16 that the system MI increases with d. This is because with the same harvested power, a larger system MI can be obtained with a better relay-receiver channel as d increases. From Figs. 15 and 16, it also can be seen that the TS protocol with no maximal transmission power limits yields a higher MI than the PS based protocol when the harvested power does not reach the bound E_m, and the latter protocol has a higher MI when the bound is approached.

To further verify the observations in Figs. 15 and 16, we plot the achievable system MI versus the average source node power P_s at various d for the three protocols in Figs. 17-19. Similar to Fig. 15, we can observe from Figs. 17-19 that the system MI first decreases and then increases with the growth of d, when the harvested energy does not reach the bound.

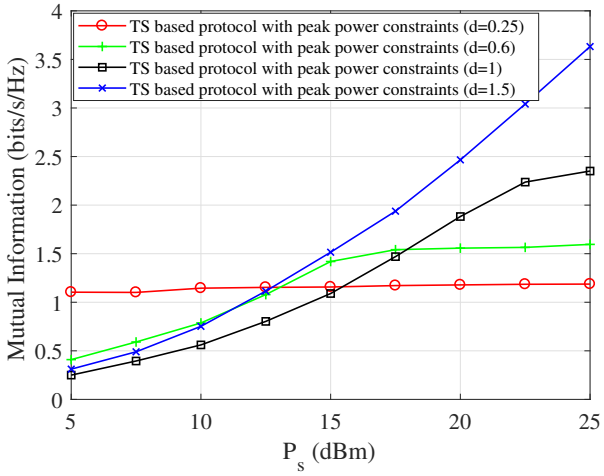

Fig. 18: Example 6: MI of the TS based protocol with peak power constraints versus P_s at various d; $N = 3$, $L = 2$, and $K = 1$.

Interestingly, when the relay node is located as $d = 1.5$, the achievable MI increases faster with P_s than that at the other three locations, as the harvested energy does not reach the bound for the E_m chosen. We can also see from Figs. 17-19 that the smaller d is, the harvested energy bound is approached at a smaller P_s. In particular, at $d = 1$, the "turning point" is around $P_s = 22$ dBm, while at $d = 0.6$, the "turning point" reduces to $P_s = 15$ dBm. At $d = 0.25$, it can be seen that the system MI almost remains constant, since the harvested energy bound is already approached for $P_s = 5$ dBm. Figs. 15-19 indicate that it is important to consider E_m when choosing the optimal location of the relay node. Theoretical analysis on the choice of the location of the relay node is shown in Appendix C.

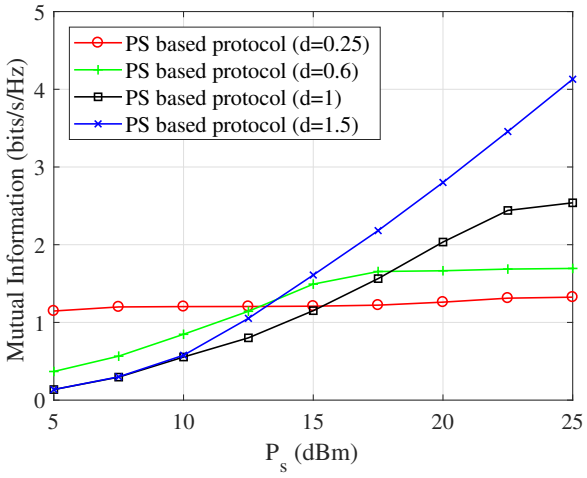

Fig. 19: Example 6: MI of the PS based protocol versus P_s at various d; $N = 3$ and $L = 2$.

G. Example 7: Achievable MI with Rician Fading Channel

In the last numerical example, we study the performance of the proposed algorithms under the Rician fading channel. The channel matrices are modelled as $\mathbf{H} = D_{sr}^{-\varsigma/2}\left(\sqrt{\frac{\kappa}{(\kappa+1)N_s}}\mathbf{1}_{N_r\times N_s} + \sqrt{\frac{1}{\kappa+1}}\bar{\mathbf{H}}\right)$ and $\mathbf{G}_l = D_{rd}^{-\varsigma/2}\left(\sqrt{\frac{\kappa}{(\kappa+1)N_r}}\mathbf{1}_{N_d\times N_r} + \sqrt{\frac{1}{\kappa+1}}\bar{\mathbf{G}}_l\right)$, $l = 1, \cdots, L$, where $\mathbf{1}_{m\times n}$ is an $m \times n$ matrix with all elements equal to 1 and κ is the Rician factor.

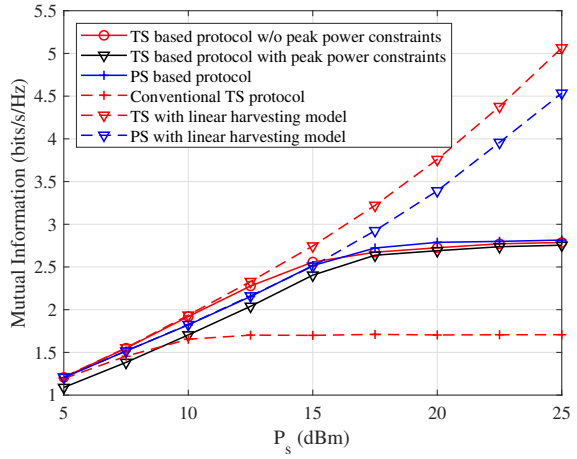

Fig. 20: Example 7: MI versus P_s; $N = 3$, $d = 1$, $L = 2$, $K = 1$, and $\kappa = 5$.

Fig. 20 shows the system MI versus P_s for $N = 3$, $d = 1$, $L = 2$, $K = 1$, and $\kappa = 5$. It can be seen that compared with Fig. 7 ($\kappa = 0$, i.e., Rayleigh fading channel), the harvested energy bound is reached at a lower P_s (17.5 dBm) for both the TS and PS based protocols. Moreover, similar to Fig. 7, we can observe from Fig. 20 that before the bound is reached, the TS based protocol without peak power constraints has a higher MI than the PS based protocol, while the latter one yields a higher MI after the bound is achieved ($P_s = 17.5$ dBm).

H. Example 8: Achievable MI at Various Noise Levels

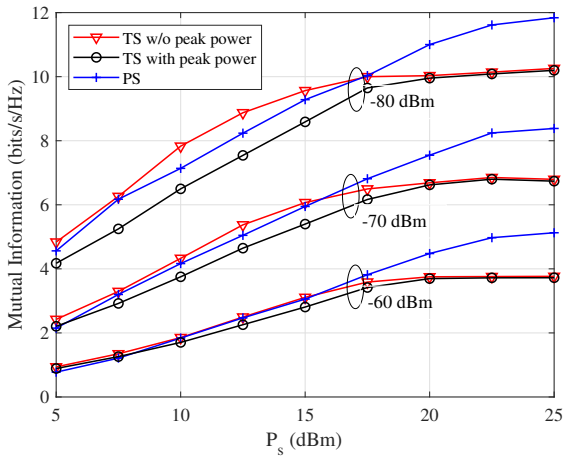

Fig. 21: Example 8: MI versus P_s at various noise levels; $N = 3$, $d = 1$, $L = 2$, and $K = 1$.

To study the impact of the noise power on the achievable system MI, we have carried out simulations with the noise power of $\sigma_r^2 = \sigma_{d,l}^2 = -60$ dBm, -70 dBm, and -80 dBm, $l = 1, \cdots, L$. It can be seen from Fig. 21 that with the decrease of the noise power, the system MI increases. Moreover, we can see that for all the three noise levels, the harvested energy bound is reached around $P_s = 22.5$ dBm. The TS based protocol without peak power constraints has a higher system MI at the low and medium P_s region, while at high P_s the PS based protocol has a higher MI. These observations imply that in practice, the noise power does not have big impact on the relative performance of the proposed algorithms.

V. Conclusions

We have considered the optimal design of the source and relay covariance matrices in a dual-hop SWIPT DF multicasting relay system and investigated the achievable system MI between the source node and multiple receivers. By introducing two additional TS factors, we have proposed a novel TS based protocol. For both the PS based protocol and the proposed novel TS based protocol, we have considered a practical nonlinear EH model at the relay node, where the harvested energy is bounded as the incident RF signal power increases. The performance of the proposed algorithms is verified by numerical simulations. Compared with the PS based protocol, the TS based protocol obtains a higher system MI when the harvested energy does not reach the bound, while the PS protocol has a higher MI when the EH circuit is saturated. For the multicasting system, the system MI decreases as the number of receivers increases. We have shown that the peak harvested energy constraint plays an important role in choosing the optimal location of the relay node.

APPENDIX A
PROOF OF THEOREM 1

It can be seen from (12) that $\mathbf{P}_1$ is not in (12a), and the value of (12a) is influenced by the feasible region of the constraint functions (12b)-(12e). Therefore, to maximize the feasible region of the problem (12), we should maximize $\mathrm{tr}(\mathbf{H}\mathbf{P}_1\mathbf{H}^H)$ for any $\mathrm{tr}(\mathbf{P}_1)$, which is given by the following optimization problem

$$\max_{\mathbf{P}_1} \ \mathrm{tr}(\mathbf{H}\mathbf{P}_1\mathbf{H}^H) \tag{31a}$$

$$\text{s.t. } \mathrm{tr}(\mathbf{P}_1) = \lambda_1, \qquad \mathbf{P}_1 \succeq 0 \tag{31b}$$

where $\lambda_1 \geq 0$. Similar to Appendix A of [5], the optimal solution of the problem (31) in terms of the EVD of $\mathbf{P}_1$ can be obtained as

$$\mathbf{P}_1^* = \lambda_1 \mathbf{v}_{h,1}\mathbf{v}_{h,1}^H. \tag{32}$$

By substituting (32) into the problem (12) and considering the limited sensitivity of the EH circuit, the optimization problem is shown as

$$\max_{\mathbf{P}_2,\mathbf{Q},\lambda_1,\alpha,\beta,\gamma} \ \mathrm{MI}(\beta,\gamma,\mathbf{P}_2,\mathbf{Q}) \tag{33a}$$

$$\text{s.t. } \beta\mathrm{tr}(\mathbf{P}_2) \leq (\alpha+\beta)P_s - \alpha\lambda_1 \tag{33b}$$

$$\gamma\mathrm{tr}(\mathbf{Q}) \leq \alpha\eta\lambda_{h,1}\lambda_1 - \gamma N_r P_c \tag{33c}$$

$$\gamma\mathrm{tr}(\mathbf{Q}) \leq \alpha E_m - \gamma N_r P_c \tag{33d}$$

$$\lambda_{h,1}\lambda_1 \geq P_t \tag{33e}$$

$$0 < \alpha,\beta,\gamma < 1, \quad \alpha+\beta+\gamma \leq 1 \tag{33f}$$

$$\lambda_1 \geq 0, \quad \mathbf{P}_2 \succeq 0, \quad \mathbf{Q} \succeq 0 \tag{33g}$$

where $\eta = \eta_1(1-\xi)$ and $E_m = (1-\xi)E_m'$. Obviously, the optimal structure of $\mathbf{P}_2$ for the problem (33) should maximize $\beta\log_2\left|\mathbf{I}_{N_r} + \sigma_r^{-2}\mathbf{H}\mathbf{P}_2\mathbf{H}^H\right|$ under the constraints of (33b) and (33g). For any feasible β, this subproblem is the same as (P2) of [5]. Therefore, the optimal structure of the above problem is

$$\mathbf{P}_2^* = \mathbf{V}_h\mathbf{\Lambda}_2\mathbf{V}_h^H. \tag{34}$$

Note that the coupling between $\mathbf{P}_1$ and $\mathbf{P}_2$ through (12b) is not affected by the structure of their EVDs in (32) and (34), since with the EVD of $\mathbf{P}_i = \mathbf{V}_i\mathbf{\Lambda}_i\mathbf{V}_i$, there is $\mathrm{tr}(\mathbf{P}_i) = \mathbf{\Lambda}_i$, $i = 1,2$. Thus, (12b) is invariant to the value of $\mathbf{V}_i$, $i = 1,2$. In fact, the coupling in (12b) is equivalently mapped to $\alpha\lambda_1 + \beta\mathrm{tr}(\mathbf{\Lambda}_2) \leq (\alpha+\beta)P_s$.

APPENDIX B
PROOF OF THEOREM 2

Firstly, the optimal form of $\mathbf{B}$ should maximize $\mathrm{tr}(\mathbf{H}\mathbf{B}\mathbf{H}^H)$ in the right-hand side of (19c), which can be written as the following optimization problem

$$\max_{\mathbf{B}} \ \mathrm{tr}(\mathbf{H}\mathbf{B}\mathbf{H}^H) \tag{35a}$$

$$\text{s.t. } \mathrm{tr}(\mathbf{B}) \leq P_s, \quad \mathbf{B} \succeq 0. \tag{35b}$$

Interestingly, the optimization problem (35) is the same as the problem (31). Thus, the optimal structure of $\mathbf{B}^*$ satisfies $\mathbf{B}^* = P_s\mathbf{v}_{h,1}\mathbf{v}_{h,1}^H$, which is a special case of $\mathbf{B}^* = \mathbf{V}_h\mathbf{\Lambda}_b\mathbf{V}_h^H$.

Secondly, the optimal $\mathbf{B}$ maximizing $\log_2|\mathbf{I}_{N_r} + \rho\sigma_r^{-2}\mathbf{H}\mathbf{B}\mathbf{H}^H|$ is also given by $\mathbf{B}^* = \mathbf{V}_h\mathbf{\Lambda}_b\mathbf{V}_h^H$ for any feasible ρ [35]. Therefore, (27) is the optimal structure of $\mathbf{B}$. Note that the optimal rank of $\mathbf{B}^*$ depends on both (19a) and (19c).

APPENDIX C
CHOICE OF THE LOCATION OF THE RELAY NODE

When the peak harvested energy constraint (22f) is active, the right-hand side of (22e) is not smaller than the right-hand side of (22f), i.e.,

$$\alpha\eta\lambda_{h,1}\lambda_1 \geq \alpha E_m \tag{36}$$

which is equivalent to

$$\lambda_{h,1} \geq \frac{E_m}{\eta\lambda_1}. \tag{37}$$

Let us introduce the SVD of $\bar{\mathbf{H}} = \bar{\mathbf{U}}_h\bar{\mathbf{\Lambda}}_h^{\frac{1}{2}}\bar{\mathbf{V}}_h^H$ and denote the first diagonal element of $\bar{\mathbf{\Lambda}}_h$ as $\bar{\lambda}_{h,1}$. From (37) and $\mathbf{H} = D_{sr}^{-\varsigma/2}\bar{\mathbf{H}}$, we have

$$D_{sr}^{-\varsigma}\bar{\lambda}_{h,1} \geq \frac{E_m}{\eta\lambda_1} \tag{38}$$

which leads to

$$D_{sr} \leq \left(\frac{\eta\lambda_1\bar{\lambda}_{h,1}}{E_m}\right)^{\frac{1}{\varsigma}}. \tag{39}$$

It can be seen from (39) that D_{sr} decreases with E_m, which means that when the maximal output power increases, the relay node should be placed closer to the source node to enable harvesting a larger amount of energy.

REFERENCES

[1] Z. Ding, C. Zhong, D. W. K. Ng, M. Peng, H. A. Suraweera, R. Schober, and H. V. Poor, "Application of smart antenna technologies in simultaneous wireless information and power transfer," *IEEE Commun. Mag.*, vol. 53, no. 4, pp. 86-93, Apr. 2015.

[2] C. Huang, J. Zhang, P. Zhang, and S. Cui, "Threshold-based transmissions for large relay networks powered by renewable energy," *IEEE Global Commun. Conf. (GLOBECOM)*, Atlanta, GA, 2013, pp. 1921-1926.

[3] X. Zhou, R. Zhang, and C. K. Ho, "Wireless information and power transfer: Architecture design and rate-energy tradeoff," *IEEE Trans. Commun.*, vol. 61, no. 11, pp. 4754-4767, Nov. 2013.

[4] L. R. Varshney, "Transporting information and energy simultaneously," *Proc. IEEE Int. Symp. Inf. Theory (ISIT)*, Toronto, ON, Canada, Jul. 2008, pp. 1612-1616.

[5] R. Zhang and C. K. Ho, "MIMO broadcasting for simultaneous wireless information and power transfer," *IEEE Trans. Wireless Commun.*, vol. 12, pp. 1989-2001, May. 2013.

[6] Y. Rong, X. Tang, and Y. Hua, "A unified framework for optimizing linear non-regenerative multicarrier MIMO relay communication systmes," *IEEE Trans. Signal Process.*, vol. 6, no. 12, pp. 4837-4851, Dec. 2009.

[7] A. A. Nasir, X. Zhou, S. Durrani, and R. A. Kennedy, "Relaying protocols for wireless energy harvesting and information processing," *IEEE Trans. Wireless Commun.*, vol. 12, no. 7, pp. 3622-3636, Jul. 2013.

[8] X. Di, K. Xiong, and Z. Qiu, "Simultaneous wireless information and power transfer for two-hop OFDM relay system," Available: http://arxiv.org/abs/1407.0166.

[9] Z. Ding, S. M. Perlaza, I. Esnaola, and H. V. Poor, "Simultaneous information and power transfer in wireless cooperative networks," *Proc. 8th Int. Conf. Commun. Netw. China (CHINACOM)*, Guilin, China, Aug. 2013, pp. 252-255.

[10] X. Yu, J. Chu, K. Yu, T. Teng, and N. Li, "Energy-efficiency optimization for IoT-distributed antenna systems with SWIPT over composite fading channels," *IEEE Internet Things J.*, vol. 7, no. 1, pp. 197-207, Jan. 2020.

[11] G. Yang, C. K. Ho, R. Zhang, and Y. L. Guan, "Throughput optimization for massive MIMO systems powered by wireless energy transfer," *IEEE J. Sel. Areas Commun.*, vol. 33, no. 8, pp. 1640-1650, Aug. 2015.

[12] X. Wang and C. Zhai, "Simultaneous wireless information and power transfer for downlink multi-user massive antenna-array systems," *IEEE Trans. Commun.*, vol. 65, no. 9, pp. 4039-4048, Sep. 2017.

[13] D. Mishra and G. C. Alexandropoulos, "Transmit precoding and receive power splitting for harvested power maximization in MIMO SWIPT systems," *IEEE Trans. Green Commun. Network.*, vol. 2, no. 3, pp. 774-786, Sep. 2018.

[14] B. K. Chalise, W.-K. Ma, Y. D. Zhang, H. A. Suraweera, and M. G. Amin, "Optimum performance boundaries of OSTBC based AF-MIMO relay system with energy harvesting receiver," *IEEE Trans. Signal Process.*, vol. 61, no. 17, pp. 4199-4213, Sep. 2013.

[15] I. Krikidis, S. Sasaki, S. Timotheou, and Z. Ding, "A low complexity antenna switching for joint wireless information and energy transfer in MIMO relay channels," *IEEE Trans. Commun.*, vol. 62, no. 5, pp. 1577-1587, May 2014.

[16] C. Zhong, H. A. Suraweera, G. Zheng, I. Krikidis, and Z. Zhang, "Wireless information and power transfer with full duplex relaying," *IEEE Trans. Commun.*, vol. 62, no. 10, pp. 3447-3461, Oct. 2014.

[17] Y. Zeng and R. Zhang, "Full-duplex wireless-powered relay with self-energy recycling," *IEEE Wireless Commun. Lett.*, vol. 4, no. 2, pp. 201-204, Apr. 2015.

[18] A. A. Nasir, H. D. Tuan, T. Q. Duong, and H. V. Poor, "MIMO-OFDM-based wireless-powered relaying communication with an energy recycling interface," *IEEE Trans. Commun.*, vol. 68, no. 2, pp. 811-824, Feb. 2020.

[19] K. Xiong, P. Fan, C. Zhang, and K. B. Letaief, "Wireless information and energy transfer for two-hop non-regenerative MIMO-OFDM relay networks," *IEEE J. Sel. Areas Commun.*, vol. 33, no. 8, pp. 1595-1611, Aug. 2015.

[20] B. Li and Y. Rong, "AF MIMO relay systems with wireless powered relay node and direct link," *IEEE Trans. Commun.*, vol. 66, no. 4, pp. 1508-1519, Apr. 2018.

[21] B. Li and Y. Rong, "Joint transceiver optimization for wireless information and energy transfer in nonregenerative MIMO relay systems," *IEEE Trans. Veh. Technol.*, vol. 67, no. 9, pp. 8348-8362, Sep. 2018.

[22] B. Li, H. Cao, Y. Rong, T. Su, G. Yang, and Z. He, "Transceiver optimization for DF MIMO relay systems with a wireless powered relay node", *IEEE Access.*, vol. 7, pp. 56904-56919, Apr. 2019.

[23] F. Benkhelifa, A. S. Salem, and M. Alouini, "Rate maximization in MIMO decode-and-forward communications with an EH relay and possibly imperfect CSI," *IEEE Trans. Commun.*, vol. 64, no. 11, pp. 4534-4549, Nov. 2016.

[24] X. Li, W. Wang, M. Zhang, F. Zhou, and N. Al-Dhahir, "Robust secure beamforming for SWIPT-aided relay systems with full-duplex receiver and imperfect CSI," *IEEE Trans. Veh. Technol.*, vol. 69, no. 2, pp. 1867-1878, Feb. 2020.

[25] D. Kudathanthirige, R. Shrestha, and G. A. A. Baduge, "Wireless information and power transfer in relay-assisted downlink massive MIMO," *IEEE Trans. Green Commun. Networking*, vol. 3, no. 3, pp. 789-805, Sep. 2019.

[26] M. R. A. Khandaker and Y. Rong, "Precoding design for MIMO relay multicasting," *IEEE Trans. Wireless Commun.*, vol. 12, pp. 3544-3555, Jul. 2013.

[27] C. Song, J. Park, B. Clerckx, I. Lee, and K.-J. Lee, "Generalized precoder designs based on weighted MMSE criterion for energy harvesting constrained MIMO and multi-user MIMO channels," *IEEE Trans. Wireless Commun.*, vol. 15, no. 12, pp. 7941-7954, Dec. 2016.

[28] E. Boshkovska, D. W. K. Ng, N. Zlatanov, and R. Schober, "Practical non-linear energy harvesting model and resource allocation for SWIPT systems," *IEEE Commun. Lett.*, vol. 19, pp. 2082-2085, Dec. 2015.

[29] K. Xiong, B. Wang, and K. J. R. Liu, "Rate-energy region of SWIPT for MIMO broadcasting under nonlinear energy harvesting model," *IEEE Trans. Wireless Commun.*, vol. 16, pp. 5147-5161, Aug. 2017.

[30] Y. J. Dong, M. J. Hossain, and J. Cheng, "Performance of wireless powered amplify and forward relaying over Nakagami-m fading channels with nonlinear energy harvester," *IEEE Commun. Lett.*, vol. 20, no. 4, pp. 672-675, Apr. 2016.

[31] L. Shi, L. Zhao, K. Liang, X. Chu, G. Wu, and H.-H. Chen, "Profit maximization in wireless powered communications with improved non-linear energy conversion and storage efficiencies," in *Proc. IEEE ICC*, Paris, France, 2017.

[32] P. N. Alevizos and A. Bletsas, "Sensitive and nonlinear far-field RF energy harvesting in wireless communications," *IEEE Trans. Wireless Commun.*, vol. 17, no. 6, pp. 3670-3685, June 2018.

[33] K. Xiong, P. Fan, Y. Lu, and K. B. Letaief, "Energy efficiency with proportional rate fairness in multirelay OFDM networks," *IEEE J. Sel. Areas Commun.*, vol. 34, no. 5, pp. 1431-1447, May. 2016.

[34] Y. Li, Y. Tian, and C. Yang, "Energy-efficient coordinated beamforming under minimal data rate constraint of each user," *IEEE Trans. Veh. Technol.*, vol. 64, no. 6, pp. 2387-2397, Jun. 2015.

[35] E. Telatar, "Capacity of multi-antenna gaussian channels," *Technical Report*, Bell Labs, 1995.

[36] N. Jindal and Z. Luo, "Capacity limits of multiple antenna multicast," *IEEE Int. Symposium Inf. Theory (ISIT)*, Seattle, WA, 2006, pp. 1841-1845.

[37] S. Boyd and L. Vandenberghe, *Convex Optimization*, New York, NY, USA: Cambridge Univ. Press, 2004.

[38] M. Grant and S. Boyd, "CVX: Matlab software for disciplined convex programming (web page and software)," Apr. 2010. Available: http://cvxr.com/cvx.

[39] K. W. Choi, D. I. Kim, and M. Y. Chung, "Received power-based channel estimation for energy beamforming in multiple-antenna RF energy transfer system," *IEEE Trans. Signal Process.*, vol. 65, pp. 1461-1476, Mar. 2017.

[40] M. Stingl, "On the solution of nonlinear semidefinite programs by augmented Lagrangian methods," Ph.D. dissertation, University of Erlangen-Nuremberg, Germany, 2006.

[41] X. Lu, D. Niyato, P. Wang, D. I. Kim, and Z. Han, "Wireless charger networking for mobile devices: Fundamentals, standards, and applications," *IEEE Wireless Commun.*, vol. 22, no. 2, pp. 126-135, Apr. 2015.

Shuche Wang received the B.Eng. and M.Sc. degree in information and communication engineering from Beijing University of Posts and Telecommunications, Beijing, China, in 2017 and 2020 respectively. His research interests include coding theory in data storage systems and signal processing in wireless communications.

Zhiqiang He (Member, IEEE) received the B.E. degree in signal and information processing and the Ph.D. degree (Hons.) in signal and information processing from the Beijing University of Posts and Telecommunications (BUPT), Beijing, China, in 1999 and 2004, respectively.

Since 2004, he has been with the School of Information and Communication Engineering, BUPT, where he is currently a Professor of the Center of Information Theory and Technology. His research interests include signal and information processing in wireless communications, networking architecture and protocol design, machine learning, and underwater acoustic communications.

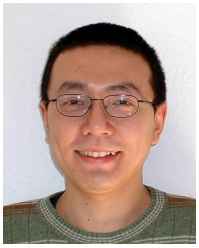

Yue Rong (Senior Member, IEEE) received the Ph.D. degree (*summa cum laude*) in electrical engineering from the Darmstadt University of Technology, Darmstadt, Germany, in 2005.

He was a Post-Doctoral Researcher with the Department of Electrical Engineering, University of California, Riverside, from February 2006 to November 2007. Since December 2007, he has been with Curtin University, Bentley, Australia, where he is currently a Professor. His research interests include signal processing for communications, wireless communications, underwater acoustic communications, underwater optical wireless communications, applications of linear algebra and optimization methods, and statistical and array signal processing. He has published over 180 journal and conference papers in these areas. He was a recipient of the Best Paper Award at the 2011 International Conference on Wireless Communications and Signal Processing, the Best Paper Award at the 2010 Asia-Pacific Conference on Communications, and the Young Researcher of the Year Award of the Faculty of Science and Engineering at Curtin University in 2010. He is a Senior Area Editor of the IEEE Transactions on Signal Processing, and was an Associate Editor of the IEEE Transactions on Signal Processing from 2014 to 2018, an Editor of the IEEE Wireless Communications Letters from 2012 to 2014, and a Guest Editor of the IEEE Journal on Selected Areas in Communications special issue on theories and methods for advanced wireless relays. He was also a TPC Member for the IEEE ICC, IEEE GlobalSIP, EUSIPCO, IEEE ICCC, WCSP, IWCMC, and ChinaCom.